doi:10.1016/j.jmb.2010.07.002 J. Mol. Biol. (2010) 401, 949–968

JMB

Available online at www.sciencedirect.com

ScienceDirect

ELSEVIER

Crystal Structure of Glyceraldehyde-3-Phosphate Dehydrogenase 1 from Methicillin-Resistant *Staphylococcus aureus* MRSA252 Provides Novel Insights into Substrate Binding and Catalytic Mechanism

Somnath Mukherjee, Debajyoti Dutta, Baisakhee Saha and Amit Kumar Das*

Department of Biotechnology, Indian Institute of Technology, Kharagpur, Pin-721302, West Bengal, India

Received 30 March 2010; received in revised form 1 July 2010; accepted 2 July 2010
Available online 8 July 2010

The dreaded pathogen *Staphylococcus aureus* is one of the causes of morbidity and mortality worldwide. Glyceraldehyde-3-phosphate dehydrogenase (GAPDH), one of the key glycolytic enzymes, is irreversibly oxidized under oxidative stress and is responsible for sustenance of the pathogen inside the host. With an aim to elucidate the catalytic mechanism and identification of intermediates involved, we describe in this study different crystal structures of GAPDH1 from methicillin-resistant *S. aureus* MRSA252 (SaGAPDH1) in apo and holo forms of wild type, thioacyl intermediate, and ternary complexes of active-site mutants with physiological substrate D-glyceraldehyde-3-phosphate (G3P) and coenzyme NAD^+. A new phosphate recognition site, "new P_i" site, similar to that observed in GAPDH from *Thermotoga maritima*, is reported here, which is 3.40 Å away from the "classical P_i" site. Ternary complexes discussed are representatives of noncovalent Michaelis complexes in the ground state. D-G3P is bound to all the four subunits of C151S.NAD and C151G.NAD in more reactive hydrate (gem-di-ol) form. However, in C151S + H178N.NAD, the substrate is bound to two chains in aldehyde form and in gem-di-ol form to the other two. This work reports binding of D-G3P to the C151G mutant in an inverted manner for the very first time. The structure of the thiaocyl complex presented here is formed after the hydride transfer. The C3 phosphate of D-G3P is positioned at the "P_s" site in the ternary complexes but at the "new P_i" site in the thioacyl complex and C1–O1 bond points opposite to His178 disrupting the alignment between itself and NE2 of His178. A new conformation (Conformation I) of the 209–215 loop has also been identified, where the interaction between phosphate ion at the "new P_i" site and conserved Gly212 is lost. Altogether, inferences drawn from the kinetic analyses and crystal structures suggest the "flip-flop" model proposed for the enzyme mechanism.

Keywords: glyceraldehyde-3-phosphate dehydrogenase; ground-state Michaelis complex; thiaocyl intermediate; new P_i site; "flip-flop" mechanism

Edited by G. Schulz

**Corresponding author.* E-mail address: amitk@hijli.iitkgp.ernet.in.

Abbreviations used: GAPDH, glyceraldehyde-3-phosphate dehydrogenase; MRSA, methicillin-resistant *Staphylococcus aureus*; SaGAPDH1, GAPDH1 from *Staphylococcus aureus* MRSA252; TmGAPDH, GAPDH from *Thermotoga maritima*; BsGAPDH, GAPDH from *Bacillus stearothermophilus*; SaGAPDH1-P_H, phosphate-bound structure of GAPDH1 in holo form from *Staphylococcus aureus* MRSA252; SaGAPDH1-P_A, phosphate-bound structure of GAPDH1 in apo form from *Staphylococcus aureus* MRSA252; r.m.s.d.C^α, root-mean-square deviation of C^α; G3P, glyceraldehyde-3-phosphate; 1,3-BPG, 1,3-bisphosphoglycerate; PEG, polyethylene glycol; PDB, Protein Data Bank.

Introduction

Staphylococcus aureus, one of the most common causes of nosocomial infections, is responsible for a wide range of illnesses from minor skin infections to life-threatening diseases such as meningitis, pneumonia, toxic shock syndrome, and septicemia. Amidst vast technical and medical advancements, it still continues to wreak havoc worldwide and remains one of the leading causes for morbidity and mortality. The resistance of this "golden staph" to all prevalent frontline antimicrobials has increased the menace. In fact, the notorious methicillin-resistant strain of *S. aureus* (MRSA) has already become an endemic in the last decade. Recent reports on the recalcitrance of this bacterium to modern glycopeptide antibiotics such as vancomycin have increased the concern to tackle the vancomycin-resistant and vancomycin intermediate *S. aureus*.[1,2]

Glycolytic enzymes, responsible for the production of ATP in the cells, are necessary for the pathogen's sustenance. The enzyme glyceraldehyde-3-phosphate dehydrogenase (GAPDH, EC: 1.2.1.12) is the sixth enzyme of the glycolytic pathway. It acts on glyceraldehyde-3-phosphate (G3P) to convert it into 1,3-bisphosphoglycerate (1,3-BPG) and consumes inorganic phosphate to harness the energy into NADH. The reaction mechanism has been intensively investigated.[3–8] Although the role of GAPDH as a housekeeping enzyme is well studied, recent investigations revealed new properties of this enzyme. These include localization on the cell surface, binding to cellular molecules,[9–14] and roles in apoptosis.[15] GAPDHs have two anion recognition sites designated as the "P_s" and the "P_i" site corresponding to the binding of substrate and inorganic phosphates. The "P_s" site is highly conserved in all eukaryotic and prokaryotic GAPDHs while location of "P_i" site varies.[16] The classical "P_i" site is found in *Bacillus stearothermophilus* while a "new P_i site" was observed in *Thermotoga maritima*. Based on the "new P_i" site, a flip-flop mechanism, in which the C3 phosphate of the substrate binds to the "new P_i" site and flips to the "P_s" site before the hydride transfer, was proposed.[17]

MRSA252 contains two cytosolic GAPDHs—GAPDH1 (National Center for Biotechnology Information accession code YP_040254) and GAPDH2 (National Center for Biotechnology Information accession code YP_041153). Because of its versatility, *S. aureus* is able to survive in extracellular or intracellular habitats, such as on skin or in epithelial cells, endothelial cells, and osteoblasts. In most of these environments, the resistance against reactive oxygen species might be important for survival. In 2004, Weber *et al.* have shown that under oxidative stress, GAPDH in *S. aureus* is irreversibly oxidized.[18] The complete inactivation of this key enzyme by oxidation was shown to have dramatic consequences of the entire catabolism of the cell, as inferred from the complete arrest in growth of the pathogen. Although sharing considerable homology with the eukaryotic GAPDHs, there is a significant difference in the mechanism and pattern of oxidation between them. Thiol oxidation of SaGAPDH is completely irreversible and totally inactivates the enzyme. However, in eukaryotic GAPDHs, S-thiolation of the catalytic cysteine protects and partially inactivates the enzyme from the oxidant. This inhibition is reversible and there is a complete resumption of activity once the oxidant is removed and the enzyme is dethiolated.[19]

Such an important enzyme such as GAPDH from *S. aureus* needs elaborate study from the structural and mechanistic aspect. Hence, this study targets the structural and functional investigation of GAPDH1 from *S. aureus* MRSA252 (SaGAPDH1).

In this study, different crystal structures of the wild-type enzyme in apo and holo forms, ternary complexes of active-site mutants with substrate and coenzyme (C151S.NAD.G3P, C151G.NAD.G3P, and C151S+H178N.NAD.G3P), and thioacyl intermediate have been described in detail with an aim to elucidate the mechanistic pathway. Structural and functional investigations of this enzyme provide novel insights into the substrate binding and catalytic mechanism. This is the very first study to report the binding of substrate in an inverted manner.

Results

Overall structure

SaGAPDH1 crystallizes in $P2_1$ space group consisting of four molecules in the asymmetric unit. The subunits, designated as O, P, Q, and R (Fig. 1a), are related by three noncrystallographic 2-fold axes of symmetry P, Q, and R with the choice of first monomer for denomination "O" being arbitrary.[20] Each of the subunit is composed of two domains: the NAD^+ binding domain (residues 1–150) and the catalytic domain (residues 151–336) (Fig. 1b). The solvent-accessible surface area of the tetrameric assembly is 44,800 Å.

The NAD^+ binding domain has a classical α/β dinucleotide binding fold—the Rossmann fold. This domain folds into nine β-sheets comprising of residues 3–8 (β_A), 27–33(β_B), 58–60 (β_C), 65–67 (β_D), 70–75 (β_E), 92–95 (β_F), 116–119 (β_G), 128–130 (β_H), and 145–146 (β_I). The strands are interconnected by either short loops or helices. β_D and the β_H runs antiparallel with the other seven parallel β-sheets. There are four helices in this domain. α_B (12–23) is in between β_A and β_B while α_C comprising of residues 38–46 connects β_B and β_C. α_D (80–88) connects β_E and β_F. α_E (103–113) is interspersed between β_F and β_G.

The catalytic domain consists of eight mixed β-strands, β_1 (170–179), β_2 (207–210), β_3 (228–235), β_4 (241–249), β_5 (271–275), β_6 (290–293), β_7 (298–302), and β_8 (305–314), and three long α-helices, α_1 (151–168), α_2 (256–266), and α_3 (317–336). The NAD^+

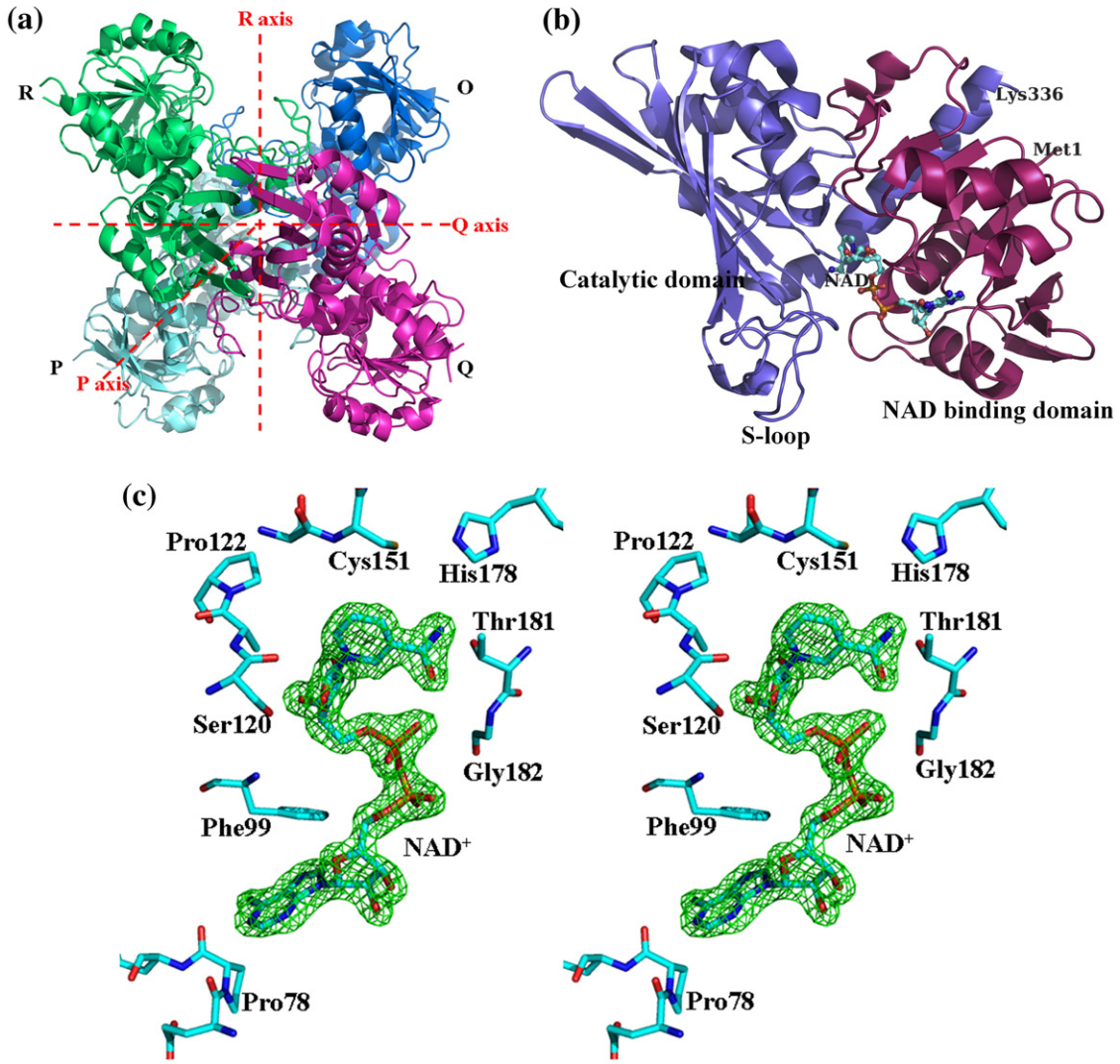

Fig. 1. SaGAPDH1—verall structure and coenzyme binding. (a) Spatial organization of the four subunits in the asymmetric unit: The subunits P (cyan), O (blue), Q (magenta), and R (green) are related by a noncrystallographic 222 symmetry on three mutually perpendicular axes designated as P, Q, and R. P-axis is orthogonal to the plane of the paper. (b) Cartoon representation of monomeric SaGAPDH1: The N-terminal domain (colored pink) binds NAD^+ (shown in sticks) while the C-terminal catalytic domain (colored blue) contains the flexible long S loop. (c) Stereoview of simulated annealing omit density map ($F_o - F_c$) of NAD^+ contoured at 3.5 σ. The unbiased omit map was calculated from the refined structure before the introduction of the coenzyme. Some of the interacting residues are highlighted.

binding domain and the catalytic domain are linked by α_1. Catalytically active residues Cys151 and His178 reside in α_1 and β_1, respectively. The C-terminal α_3 helix (317–336) fits into a groove of the N-terminal domain and is involved in a number of interactions with the coenzyme. A prominent feature of the catalytic domain is a large S-shaped loop called "S loop" comprising of residues 179–206. The flexible nature of this long unstructured region is evident from its comparatively high temperature factor values and poorly defined electron density maps for some residues in some of the subunits.

Superimposition of the NAD^+ binding domain of the P subunit of SaGAPDH1 with that of GAPDH from *T. maritima* (TmGAPDH) [Protein Data Bank (PDB) code: 1HDG, sequence identity: 53%][21] gives a root-mean-square deviation of C^α (r.m.s.d.C^α) of 0.64 Å. C^α (1–151) was used to calculate the superposition matrix. Insignificant differences are observed in the helices and strands while the variations in loop regions (139–143) are noticeable. When superposed with catalytic domain of a monomer of 1HDG, r.m.s.d.C^α (152–332) of the catalytic domain of the P subunit is quite high (1.09 Å). This can be accounted for a substantial variation not only in the orientation of flexible loops but also in orientations of more ordered α-helices and β-strands that occur due to insertions and deletions. The S loop is primarily responsible for the intersubunit interactions. The structures of SaGAPDH1 presented in this article are within the range of expected stereochemical parameters (Table 1).

Table 1. Summary of data collection and refinement statistics

					Ternary complex			
	Holo	Apo	Holo_PO4 (SaGAPDH1-P_H)	Apo_PO4 (SaGAPDH1-P_A)	C151S.NAD. G3P	C151G.NAD. G3P	C151S+H178N. NAD.G3P	Thioacyl complex
Data collection								
Space group				$P2_1$				
Cell parameters								
a, *b*, *c* (Å)	68.2, 104.9, 91.2	64.3, 94.9, 86.6	68.2, 104.9, 90.6	67.0, 93.7, 89.1	68.5, 104.5, 91.2	68.6, 103.0, 90.7	67.9, 93.9, 89.9	69.1, 103.0, 90.3
β (°)	107.7	105.7	107.6	106.8	108.0	109.3	107.6	109.4
Resolution (Å)	30.78–1.70 (1.76–1.70)	19.65–2.50 (2.63–2.50)	19.14–2.50 (2.59–2.50)	33.34–2.20 (2.28–2.20)	21.35–2.50 (2.59–2.20)	27.28–2.20 (2.28–2.20)	33.83–2.60 (2.69–2.60)	19.91–2.80 (2.94–2.80)
Completeness (%)	94.5 (93.6)	99.3 (96.7)	99.8 (99.7)	99.7 (97.3)	98.8 (97.7)	99.6 (98.4)	99.0 (90.4)	99.2 (96.9)
Redundancy	3.5 (3.4)	3.7 (3.5)	3.0 (2.9)	3.6 (3.3)	3.7 (3.7)	3.6 (3.5)	3.6 (3.2)	3.8 (3.7)
$I/\sigma(I)$	8.7 (2.4)	19.1 (4.5)	8.1 (2.5)	6.8 (2.3)	9.7 (3.2)	8.3 (2.5)	7.4 (2.4)	9.8 (2.7)
R_{merge} (%)[a]	5.9 (43.0)	6.1 (28.1)	8.5 (37.6)	8.8 (42.8)	8.4 (34.4)	8.3 (40.7)	10.0 (38.9)	13.4 (49.7)
Refinement								
Resolution (Å)	20.00–1.70	20.00–2.50	19.14–2.50	20.00–2.20	21.35–2.50	27.26–2.20	33.83–2.60	20.00–2.80
No. of reflections	126,514	34,621	41,927	53,279	41,750	57,048	32,754	29,373
R_{work} (%)[b]	18.9	18.7	17.7	21.6	18.7	19.7	20.0	18.1
R_{free} (%)[b]	22.1	24.9	22.4	25.8	23.8	24.9	24.8	24.1
Average *B*-factors (Å^2)								
Protein	32.2	26.0	45.8	52.5	26.3	23.5	36.9	23.3
NAD	39.0	—	43.9	—	30.5	24.7	37.0	—
G3P	—	—	—	—	64.1	38.2	71.0	31.5
Phosphate	—	—	84.0	67.0	—	—	—	—
Glycerol	—	—	—	—	—	—	—	31.1
Chloride	—	—	—	—	—	—	—	43.0
Water	34.9	28.0	47.9	54.6	28.4	25.9	39.06	25.4
r.m.s.d.								
Bond length (Å)	0.006	0.014	0.015	0.014	0.015	0.017	0.014	0.013
Bond angle (°)	1.04	1.57	1.55	1.47	1.57	1.70	1.50	1.43
Ramachandran plot (%)								
Most favored	91.1	88.0	90.1	89.9	88.7	88.7	88.5	88.6
Additionally allowed	8.7	11.2	9.9	10.0	11.1	10.9	11.2	11.3
Generously allowed	0.3	0.4		0.1	0.2	0.3	0.3	0.1

Values in parentheses correspond to values in the highest-resolution shell.

[a] *R*-factor for symmetry-related intensities.

[b] R_{work} is crystallographic *R*-factor. R_{free} is calculated based on 5% of total reflections excluded from refinement.

All the subunits within each asymmetric unit are structurally similar as inferred from the r.m.s.d.C^{α} values. However, the tetramers generated by the noncrystallographic 222 symmetry have three nonequivalent interfaces. The P-axis interface (between subunits O and P and subunits R and Q) is the most extended interface (2058 Å^2) and is principally formed by the β-strands and the S loop. The R-axis interface (between subunits O and R and subunits P and Q) is smaller (1365 Å^2), and finally, the Q-axis interface (between subunits O and Q and subunits R and P) extend only through 518 Å^2. The most extended subunit interactions are formed by the P-axis-related monomers, with 58

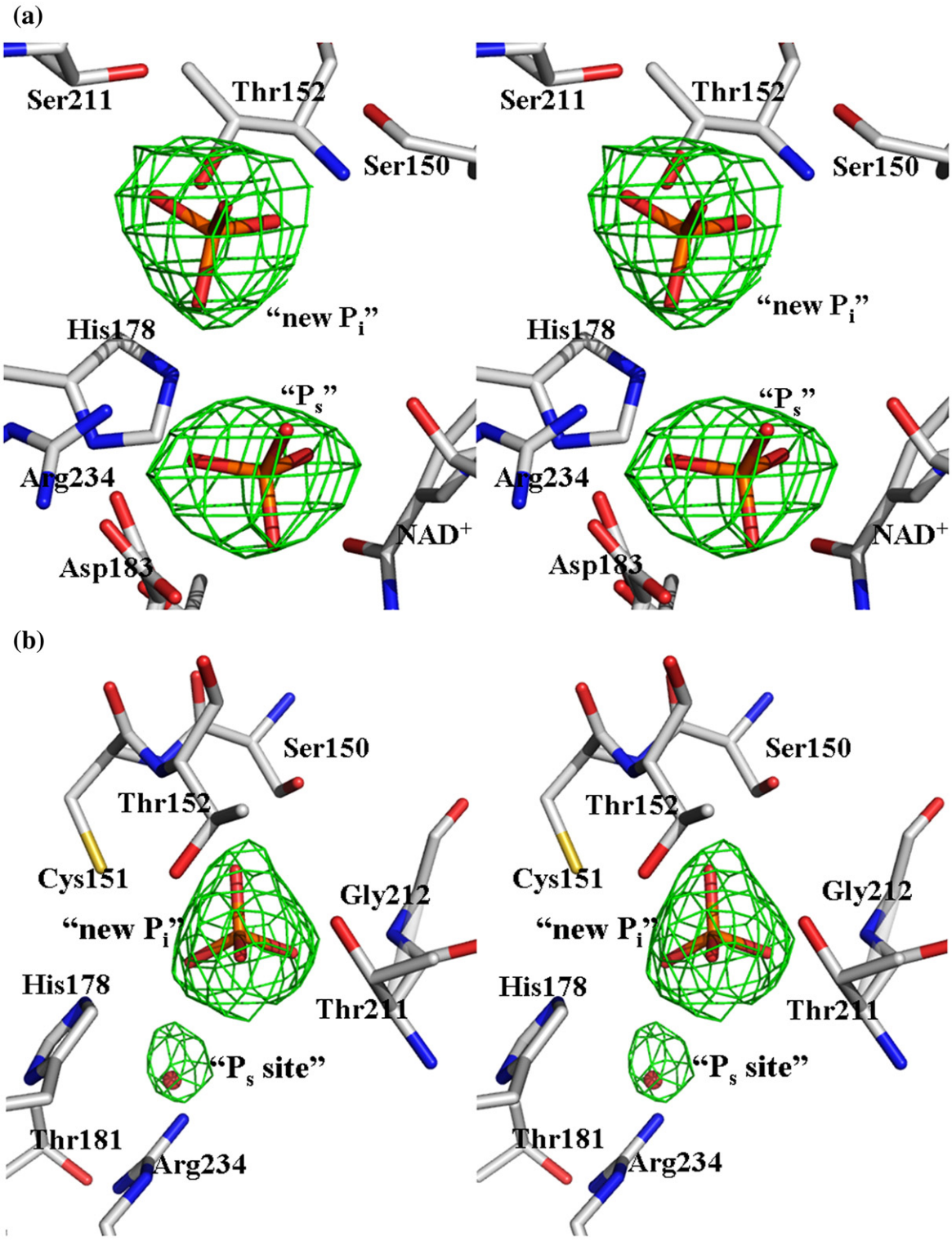

Fig. 2 (*legend on page 955*)

residues per subunit interacting less than 4.0 Å distance from an atom in the adjoining subunit. About 40 hydrogen bonds and 30 salt bridges between the different polar residues along the interface are observed.

Coenzyme binding

NAD^+ was not added during the entire purification and crystallization process, but during restrained refinement of the initial model of holoen-

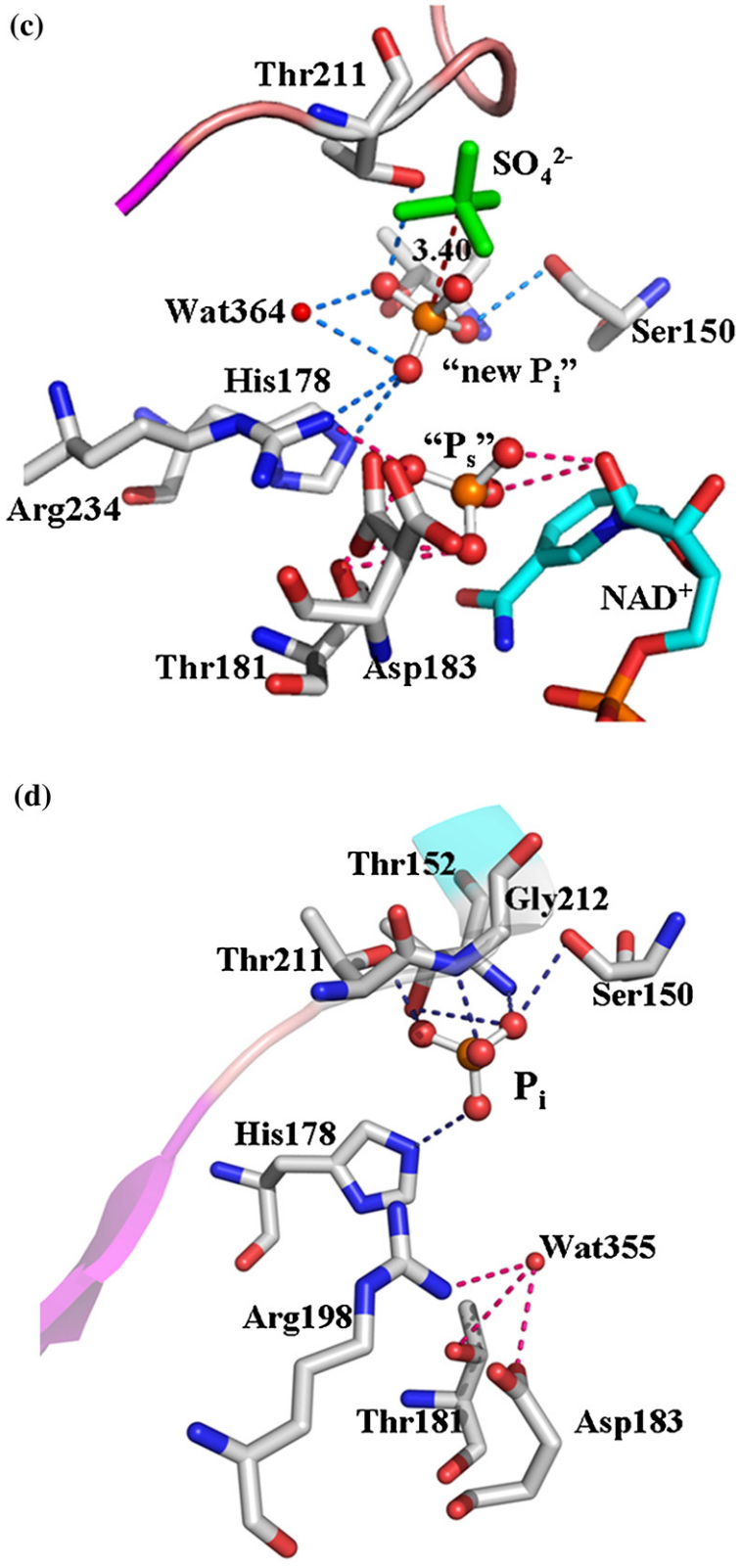

Fig. 2 (*legend on next page*)

zyme, a strong peak in the F_o-F_c omit map corresponding to 10 σ (Fig. 1c) was observed in each of the subunit that can only be accounted for the incorporation of the coenzyme. During overexpression in *Escherichia coli*, the heterologous protein consumes its coenzyme from the host cells. In all other GAPDHs reported so far in the literature, the purified recombinant enzyme is principally obtained in the apo from. SaGAPDH1 is the first of its kind that was overexpressed and purified with its bound coenzyme. In all the four subunits, it sits in the groove of the N-terminal domain, in an extended conformation with the nicotinamide ring pointing towards the catalytic Cys151 and His178, and possesses average temperature factors similar to those of the protein. Containing polar ribose and phosphate units, the coenzyme is principally stabilized by salt bridges and hydrogen bonds with neighboring polar amino acid residues and solvent molecules (Supplementary Fig. 1). Pi stacking interaction is observed between the aromatic side chain of Tyr320 and the nicotinamide ring of NAD^+ lying in parallel orientation. The C4 of the nicotinamide ring is positioned at a distance of 5.89 and 3.93 Å from the imidazole NE2 of the His178 and SG of Cys151, respectively. His178 and Cys151, along with NAD^+, form the perfect pocket for the substrate binding.

Phosphate binding: "P_s" and "new P_i" site

SaGAPDH has two anion recognition sites designated as "P_s" and "new P_i" site that correspond to the binding of the C3 phosphate of G3P and inorganic phosphate required for phosphorylation. We have separately crystallized the enzyme in the presence of phosphate in both holo (SaGAPDH1-P_H) and apo (SaGAPDH1-P_A) forms. Analysis of the unbiased F_o-F_c omit maps (Fig. 2a and b) of SaGAPDH1-P_H and SaGAPDH1-P_A clearly revealed peak of electron density above 5 σ corresponding to the anions. In SaGAPDH1-P_H, all the "P_s" and "P_i" sites of the four chains contain phosphate ions with full occupancy. The "P_s" site is composed of the side chains of the residues of Asp181, Thr183, and Arg234 and the 2′ hydroxyl (O2D) of the ribose unit attached to the nicotinamide ring of NAD^+ (Fig. 2c). The "P_i" phosphate is principally stabilized by the side chains of conserved Thr211, Ser150, His178, and Arg234 and the main-chain nitrogen and side-chain hydroxyl of Thr152. The position of the "P_i" phosphate is quite different from that of the "classical P_i" site but similar to that found in TmGAPDH[21] and is generally referred to the "new P_i" site. It is situated closer to the catalytic Cys151. A number of water-mediated hydrogen-bonding interactions with polar side-chain groups of amino acid residues also stabilize the phosphate ion in this new hydrophilic pocket. This "new P_i" site in SaGAPDH1 is 3.40 Å away from the "classical P_i" site obtained in GAPDH from *B. stearothermophilus* (BsGAPDH) (1GD1, sequence identity: 50%)[17] (Fig. 2c). The presence of phosphate ion in the "classical P_i" site or in the "new P_i" site depends upon the conformation of the strand–loop–helix segment containing the residues 209–215 in SaGAPDH1. This segment corresponds to residues 206–212 in other GAPDHs where it is commonly referred to as the "206–212 loop".

SaGAPDH1-P_A has fully occupied "new P_i" sites in the four subunits but a totally empty "P_s" site (Fig. 2d). The "P_s" site is occupied with water molecules. The position of "P_i" phosphate is identical with that obtained in holoenzyme. An additional interaction appears in SaGAPDH1-P_A between one of the oxygen atoms of the "P_i" phosphate and the main-chain nitrogen of Gly212. This arises due to slight rearrangement of the 209–215 loop that pushes the amide nitrogen of Gly212 3.30 Å more towards the "new P_i" site.

Structures of ternary complexes

Superposition of each of the ternary complexes (C151S.NAD.G3P, C151G.NAD.G3P, and C151S+H178N.NAD.G3P) with its corresponding binary complexes gives r.m.s.d.C^α of less than 0.15 Å, which proves that no drastic conformational change has been introduced upon substrate binding. Analysis of unbiased F_o-F_c maps of the three ternary complexes clearly shows a strong peak of electron density above 8 σ in the active site that can be attributed to bound substrate.

The substrate is bound in a noncovalent manner in all the three complexes. Overall *B*-factors of G3P are comparatively higher due to exposed active-site cavity. In C151S.NAD.G3P and C151S+H178N.NAD.G3P, G3P is bound to all the subunits with

Fig. 2. Phosphate binding to SaGAPDH1. Stereoview of the unbiased simulated annealing (F_o-F_c) omit maps (contoured at 3.5σ) of phosphate binding sites in (a) SaGAPDH1-P_H and (b) SaGAPDH1-P_A. In (a), both the "P_s" and "new P_i" sites are occupied by phosphate ions while in (b), only the "new P_i" site is occupied by phosphate. Water molecules reside in the "P_s" site. The maps were computed before the phosphate ions were introduced. (c) Phosphate ions bind to both the "P_s" and the "new P_i" site in all four chains of SaGAPDH1-P_H. Selected stabilizing interactions of the "P_s" phosphate and "new P_i" phosphate with amino acid residues and solvent molecules are shown in pink and blue, respectively. The sulfate ion residing in the "classical P_i" site in BsGAPDH (PDB code: 1GD1) is overlaid on the structure of the SaGAPDH1-P_H. The "new P_i" site in SaGAPDH1-P_H is 3.4 Å away from the "classical P_i" site in BsGAPDH. The figure shown corresponds to the Q subunit of SaGAPDH1-P_H. (d) Phosphate ions bind only to the "new P_i" site in all the four subunits of SaGAPDH1-P_A. The "P_s" site is filled by water molecules in all the four chains. Interactions of the protein atoms with the "P_i" phosphate is highlighted in blue while those with water molecule in the "P_s" site are shown in pink. Additional interaction arises between the amide nitrogen of Gly212 and the "P_i" phosphate due to movement of the 209–215 segment (shown in cartoon). The figure corresponds to the R chain of SaGAPDH-P_A.

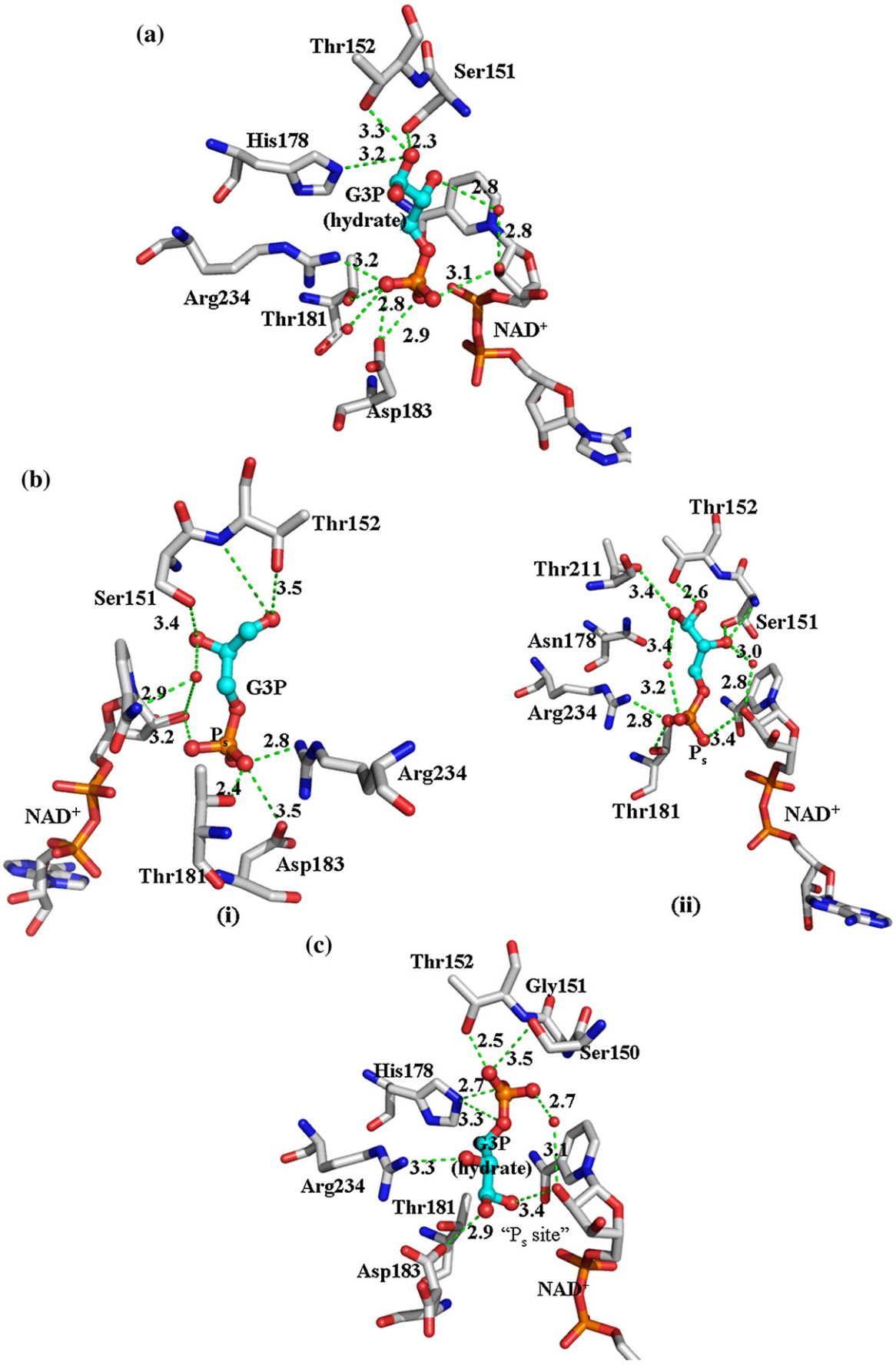

Fig. 3 (*legend on next page*)

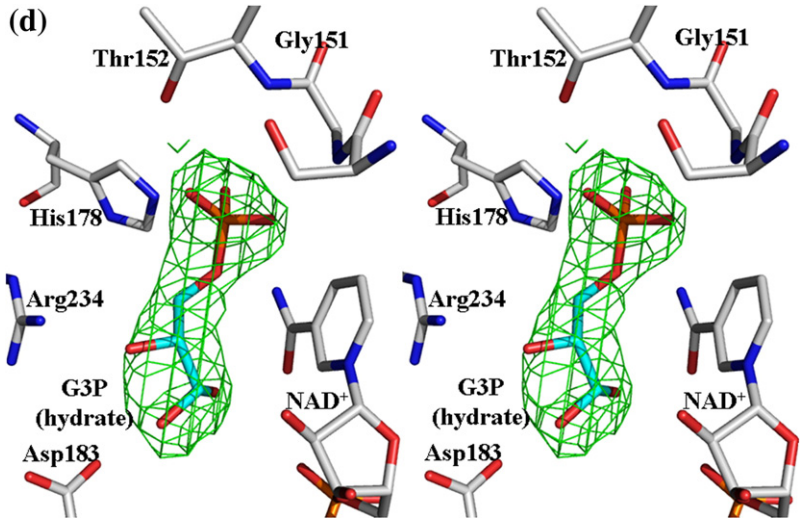

Fig. 3. Active sites of ground-state Michaelis complex: (a) C151S.NAD.G3P (Chain O): G3P is in hydrated gem-di-ol form. (b) C151S + H178N.NAD.G3P (i) Chain O: G3P is in aldehyde form. (ii) Chain Q: G3P in hydrated gem-di-ol form. (c) C151G.NAD.G3P (Chain P): G3P is in gem-di-ol form. The C3 phosphate of G3P is positioned in the "P_s" site of (a) and (b) while the "new P_i" site remains unoccupied. G3P binds in a completely inverted manner in (c). Here, C1 of G3P resides in the "P_s" site. Some of the polar interactions (shown in green) of G3P with amino acid residues, NAD^+, and water molecules are highlighted. (d) Stereoview of simulated annealing ($F_o - F_c$) omit map of G3P in C151G.NAD.G3P justifies the inverted orientation of substrate. The map is contoured at 3.5 σ and is computed before the introduction of the substrate. G3P is shown in gem-di-ol form.

its C3 phosphate positioned in the "P_s" site while the "new P_i" site remains unoccupied (Fig. 3a and b). This is similar to that observed in the ground-state Michaelis complexes from *B. stearothermophilus* but in contrast to GAPDH from *Cryptosporidium parvum* (PDB code: 3CIF, sequence identity: 46%)[22] where the C3 phosphate is bound to the "new Pi" site in three of the four subunits and in a completely different position in the fourth. The oxygen atoms of the C3 phosphate (O1P, O2P, O3P, and O4P) form extensive hydrogen bonds with the side chains of conserved Thr181, Asp183, and Arg234 and with the 2′ hydroxyl group of ribose (O2D) adjacent to the nicotinamide group of NAD^+. The H-bonding interaction between the O1A atom of G3P and NE2 of His178 that is present in C151S.NAD.G3P (Fig. 3a) is lost in the ternary complex of double mutant (Fig. 3b).

In C151G.NAD.G3P, G3P binds in a completely inverted manner with its C3 phosphate positioned in the cavity lined by Ser150, Gly151, and Thr152 (Fig. 3c). Placing the substrate with its C3 phosphate in the "P_s" site in unbiased $F_o - F_c$ map resulted in improper fitting of the ligand with some unresolved negative density over the "P_s" site. However, placement of G3P in the reverse manner with the C1 atom positioned in the "P_s" site solved the problem. The difference electron density map of bound G3P is shown in Fig. 3d. Several reasons can be put forward to explain this interesting but apparently contradictory observation. Firstly, mutation of Cys151 to a glycine residue increases the size of the active-site cavity by almost 10.0 $Å^3$ that gives enough space to G3P to be accommodated in an inverted manner. Secondly, although some of the interactions between the enzyme and the ligand are compromised, some additional hydrogen-bonding interactions of oxygen atoms of C3 phosphate group with the side chains and peptide backbone of the enzyme can be principally inferred to localize C3 phosphate in this new orientation. The O1A, O1B, and O2 in turn are hydrogen bonded to the side chains of Asp183, Arg234, and the 2′ hydroxyl group of the ribose (O2D) of the coenzyme (Fig. 3c).

In spite of using D,L-G3P in the soaking experiments, the C2 carbon adopts an R configuration, which accounts for greater affinity of the enzyme towards D-G3P. In C151S_G3P and C151S + H178N_G3P, the C2 hydroxyl group of G3P is stabilized by hydrogen bonds with OG side chain and amide nitrogen of Ser151. Moreover, an additional stabilization may arise due to the interaction of C2–OH with a water molecule that is stabilized through hydrogen bonding to O2D and N7N of NAD^+ (Fig. 3a and b).

In the complexes C151S.NAD.G3P and C151G.NAD.G3P, G3P is bound in hydrate (gem-di-ol) form to all the four subunits. This is not unlikely because the equilibrium between the aldehyde and gem-di-ol form (Fig. 4a) is strongly shifted towards the latter in solution and the proportion of the hydrate form increases with electron-withdrawing substituents. G3P has an electron-withdrawing hydroxyl and phosphate group that can stabilize the di-ol form significantly. The observation is similar to that observed in the case of C149A mutant of *E. coli* that uses the hydrate form of substrate.[23] However, in the ternary complex of double mutant, the substrate is bound to two

chains in aldehyde form (O and R) (Fig. 3b, i) and in gem-di-ol form to the other two (P and Q) (Fig. 3b, ii). Analysis of simulated annealing $F_o - F_c$ omit maps (Fig. 4b and c) allows us to place the substrate unambiguously in the required form within the active-site cavity of different subunits. A careful analysis of the interactions that can principally stabilize the hydrated form with respect to the free aldehyde form clearly reveals the role of His178. A hydrogen bond between O1A of G3P and NE2 of His178 at a distance of 2.65 Å in C151S.NAD.G3P is one such stabilizing interaction that is lost in the ternary complex of the double mutant. Absence of such an important interaction may be postulated to shift the equilibrium more towards the aldehyde form. Some subtle differences between the structures of SaGAPDH1 and BsGAPDH[24] may be responsible for the substrate to exist in two different forms in these two enzymes that however remain inexplicable because

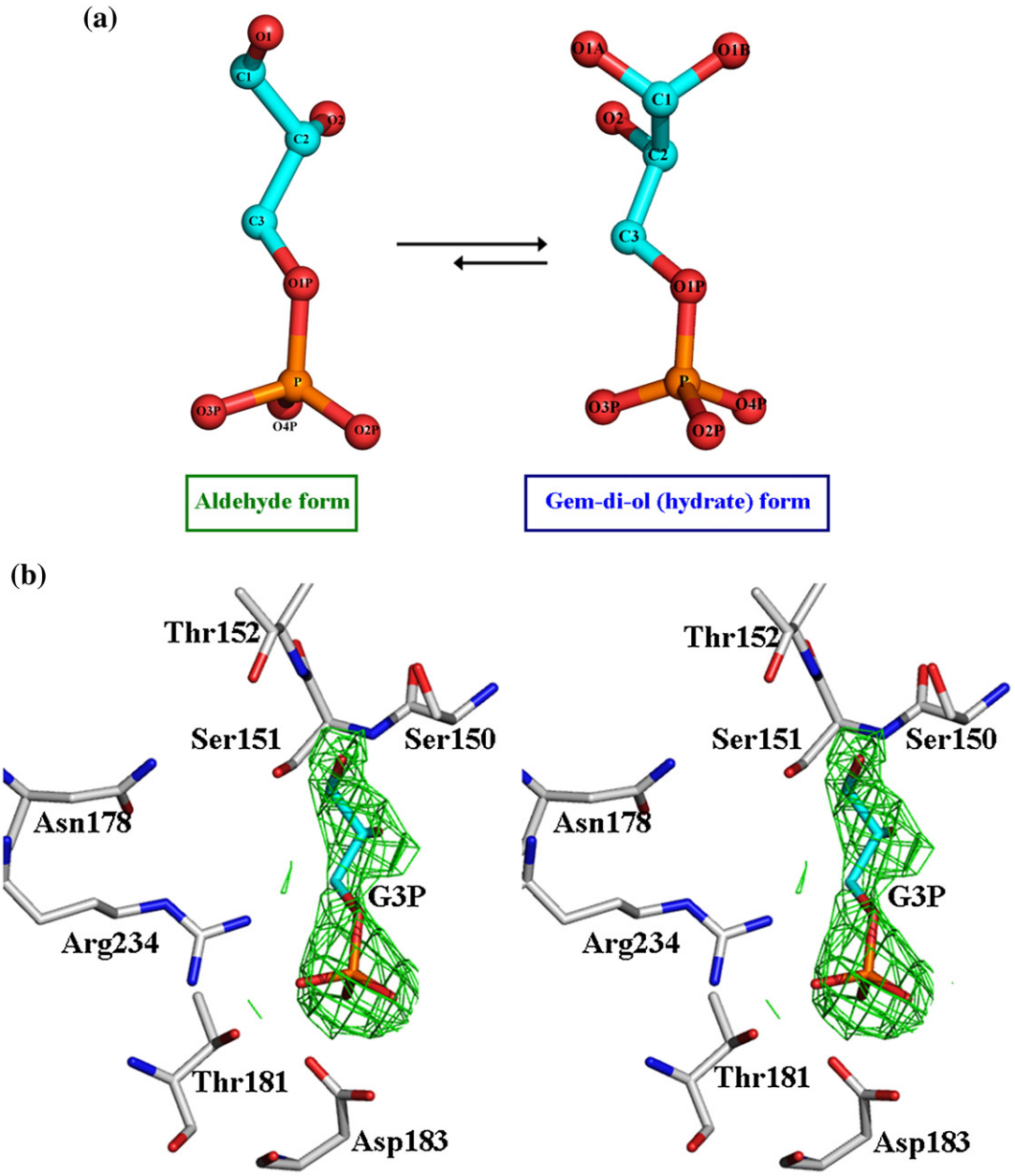

Fig. 4. Views of D-G3P molecule. (a) Equilibrium between the aldehyde and hydrate (gem-di-ol) form of D-G3P. The equilibrium is strongly favored towards the hydrated form in aqueous solution owing to extensive hydrogen bonding. C2 is chiral and is in "R" configuration. O1 and O2 point in the opposite direction. The atomic numbering of D-G3P used in this article is depicted here. Stereoview of simulated annealing $F_o - F_c$ map of D-G3P in (b) aldehyde form and (c) gem-di-ol (hydrate) forms found in C151S + H178N.NAD.G3P.The unbiased difference maps are calculated before the introduction of the substrate (contour level, 3.5 σ). C1 of D-G3P (hydrate form) depicted here is tetrahedral with one hydrogen and two oxygen atoms. Some of the interacting residues are highlighted.

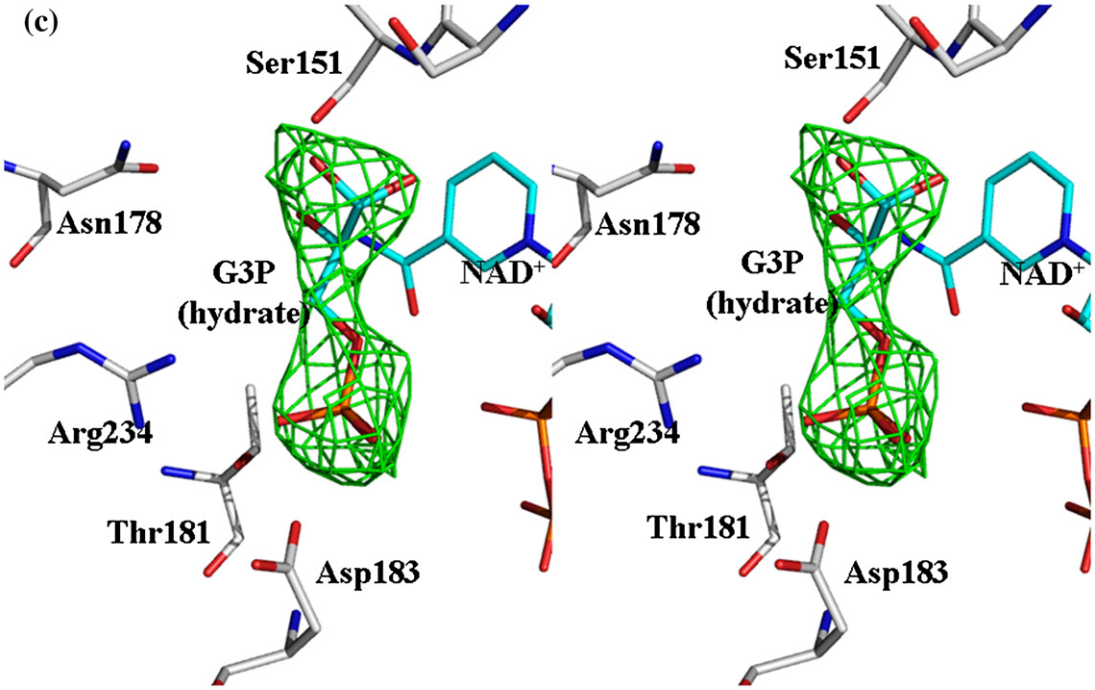

Fig. 4 (*legend on previous page*)

the active-site residues and geometry are more or less conserved.

The absence of a covalent bond formation between C1of D-G3P and Ser151 is justified from a kinetic point of view. The rate of acylation is decreased by 23,000 times when the active-site Cys151 is mutated to serine. In the crystallization medium containing polyethylene glycol (PEG) 4000, the acylation rate is probably even more retarded than in aqueous solution, which helps the noncovalently bound G3P to be stable in the ternary complex even after soaking with 50 mM G3P for 10 min.

Structure of thioacyl intermediate

The mechanism of oxidative phosphorylation proceeds via a thioacyl intermediate. We were able to isolate the intermediate in the case of apoenzyme, but it was not possible to trap such an intermediate in the case of holoenzyme as the reaction was instantaneous. G3P binds to the catalytic site in all the four chains. Unbiased difference map of the thioacyl intermediate is shown in Fig. 5a. Although noncrystallographic restraints were not imposed on the substrate, it essentially binds to all the four monomers with identical conformations sharing almost similar interactions. The thioester bond is formed between the sp^2 hybridized C1 of G3P and SG of catalytic Cys151 (Fig. 5b). The phosphate group is now positioned in the "new P_i" site in contrast to the "P_s" site as found in the ternary complexes of the mutant proteins. The "new P_i" site is positioned at a distance of 6.0 Å from the "P_s" site. Phosphate group in the "new P_i" site is stabilized by a number of hydrogen-bonding interactions with side-chain and main-chain atoms of conserved His178 and Thr211, respectively, and guanidium group of Arg234 via a water molecule. This shift of the C3P group from "P_s" to "new P_i" site is associated with a significant rearrangement of the carbon chain of the ligand. While O1 is oriented towards His178 in the ternary complexes, it points away from catalytic histidine in the thioacyl intermediate (Fig. 5c). It is observed that the C2-O2 bond in the thioacyl intermediate is parallel with the plane of the nicotinamide ring of the coenzyme but is oriented perpendicularly in the ternary complex.

The preferential uptake of the D isomer by the enzyme can be explained from the structure of the thioacyl complex. In the case of D-G3P, the intermediate clearly shows that C1 and C2 of the phosphoglycerol moiety both adopt an R configuration that places O1 atom trans to O2 (Fig. 5a). In the case of L-G3P, the S configuration of C2 orients O1 and O2 cis to each other. The two hydroxylic groups then are sufficiently close to make an H-bonding interaction that can stabilize the cis conformation, but the Pitzer (torsional) strain developed due to their dihedral angle makes the overall interaction unfavorable. The lower energy associated with trans conformation explains the higher affinity of the enzyme towards D-G3P.

Conformations of the 209–215 loop in comparison to other GAPDH structures

In all the structures of SaGAPDH1 discussed, the 209–215 loop exists in two conformations—Conformation I and Conformation II (Fig. 6a). Conformation

I is present in the all the structures of SaGAPDH1 except in SaGAPDH1-P_A and thioacyl intermediate where it adopts the alternate Conformation II. Conformation I is more equivalent to Conformation A and Conformation II is identical with Conformation B of the 206–212 loop in thioacyl intermediate of BsGAPDH (3CMC).[25] C^{α} of Gly212 in Conformation I of SaGAPDH1-P_H is at a distance of 2.80 Å from the corresponding C^{α} of Gly209 in Conformation B (BsGAPDH) but only away by 0.80 Å in Conformation A (BsGAPDH). In the thioacyl intermediate of BsGAPDH, the loop in Conformation A stabilizes the sulfate ion (from crystallization medium) in "classical P_i" site while the loop in Conformation B stabilizes the

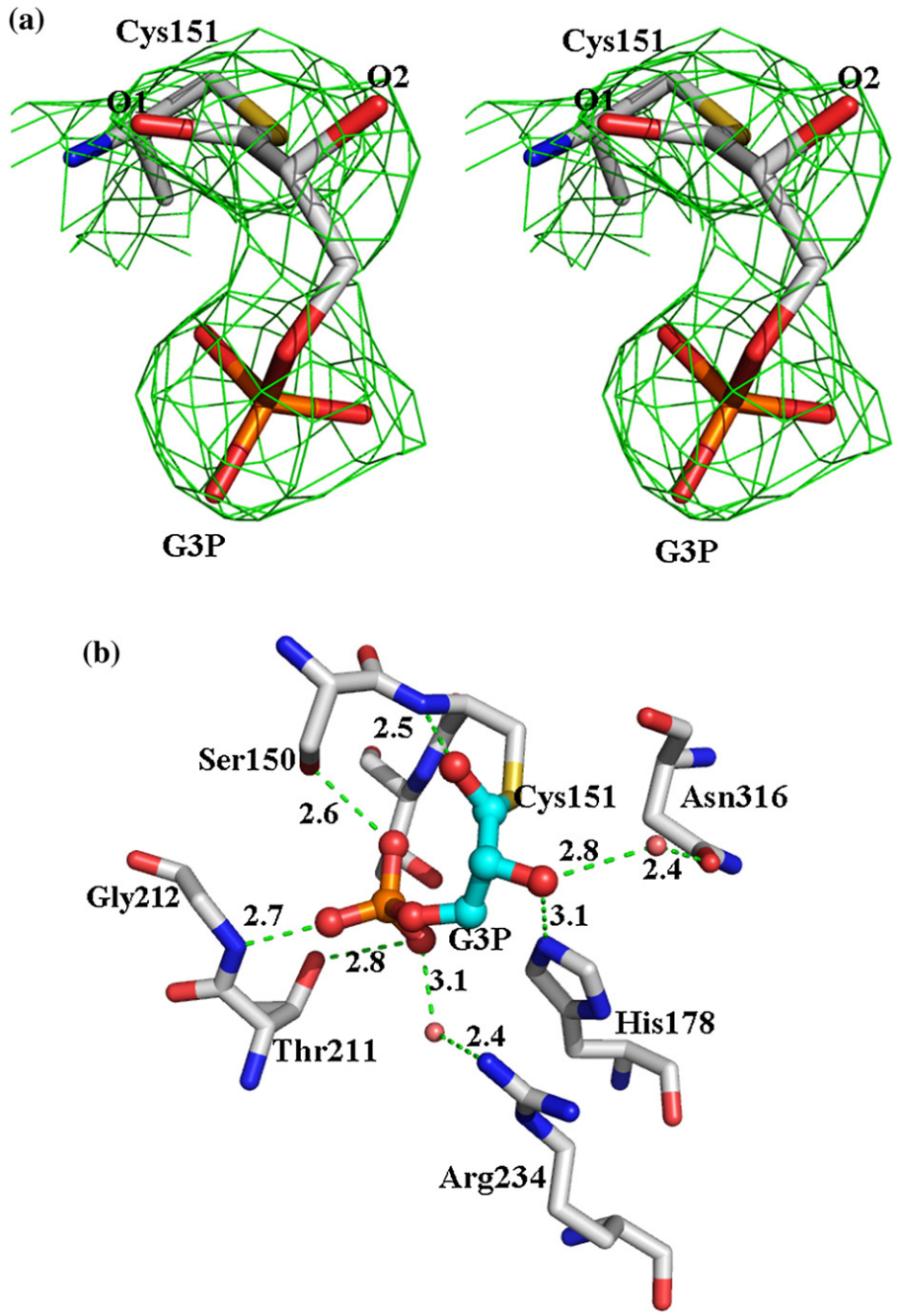

Fig. 5. Structure of thioacyl intermediate. (a) Stereoview of simulated annealing omit ($F_o - F_c$) map of the thioacyl intermediate contoured at 3.5 σ. Trans orientation of O1 and O2 is retained in the complex. (b) Active site of thioacyl complex. C1 of D-G3P is sp^2 hybridized and the C3 phosphate is bound to the "P_i" site. Selected stabilizing interactions are highlighted in green. (c) Superimposition of the active site of the thioacyl complex (R subunit) with that of the ternary complex C151S.NAD.G3P. The thioacyl complex is shown in green while the ternary complex is colored magenta. The C3 phosphate of G3P is positioned in the "P_s" site in the ternary complex but is flipped to the "P_i" site in the thioacyl complex. Flipping of the C3 phosphate orients the C1–O1 bond away from the catalytic His178.

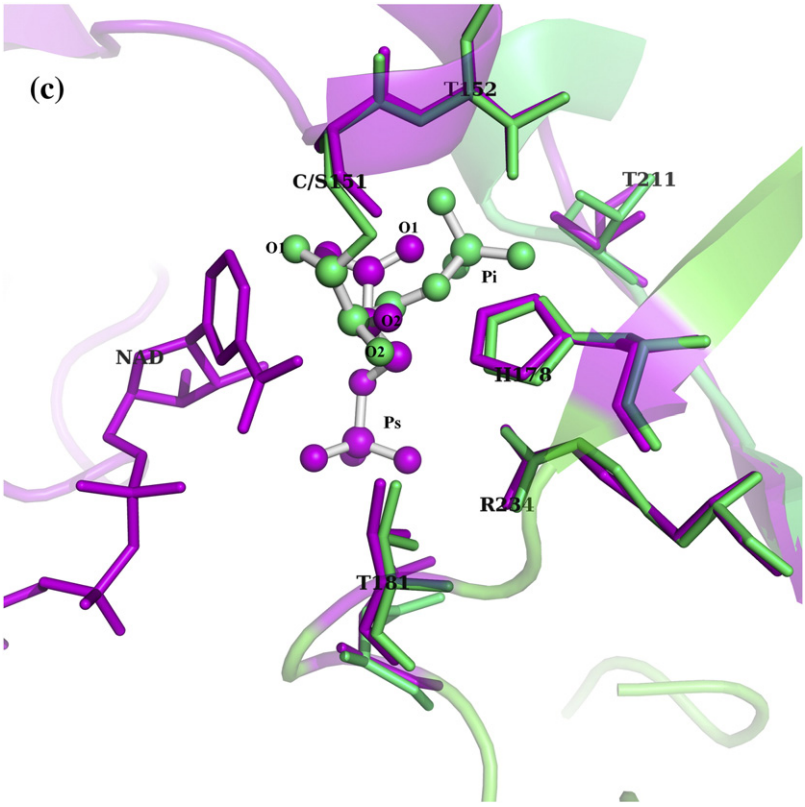

Fig. 5 (*legend on previous page*)

C3 phosphate of the intermediate in the "new P_i" site. However, in SaGAPDH1-P_H, phosphate is bound in the "new P_i" site although the 209–215 loop is in Conformation I. In fact, superimposition of the main-chain atoms of the O subunit of SaGAPDH1-P_H with the hemithioacetal intermediate from GAPDH from *E. coli* (PDB code: 1DC4, sequence identity: 47%),[26] thiaocyl complex of BsGAPDH (PDB code: 3CMC),[25] and TmGAPDH (PDB code: 1HDG)[21] shows that the central phosphorus atom of the "P_i" phosphate at the "new P_i" site in SaGAPDH1 is only 0.40 Å away from others. This obviously raises the question whether the stabilizing interactions between the phosphate ion in the "new P_i" site and residues of the loop in Conformation B found in other GAPDHs still remain unperturbed in SaGAPDH1-P_H where the loop is present in Conformation I. Conformation I in SaGAPDH1-P_H is similar but not "strictly equivalent" to the Conformation A in BsGAPDH. A closer inspection in the structure of SaGAPDH1-P_H reveals that the loop in Conformation I actually lies in between Conformations A and B found in the thioacyl complex of BsGAPDH, more towards Conformation A than B (Fig. 6b). Gly212 C^{α} is shifted by 1.0 Å towards catalytic Cys151. Contrary to other GAPDHs, the polar interaction between the backbone nitrogen of conserved Gly212 and phosphate ion in the "new P_i" site is lost in SaGAPDH1-P_H. The disposition of the loop in Conformation I in SaGAPDH1-P_H shifts nitrogen of Gly212 2.30 Å outward in comparison to that of Gly209 (Conformation B) in the acyl complex of BsGAPDH. This outward movement of Gly212 is responsible for loss of this interaction. The "P_i" phosphate is, however, stabilized by interaction with water molecules and polar side-chain residues.

Kinetic analyses

The pH optimum and the temperature for the maximum activity of the wild-type SaGAPDH1 are 8.7 and 25 °C. The kinetic parameters are listed in Table 2 and the corresponding Michaelis–Menten plots are shown in Supplementary Fig. 2. Mutation of the catalytically active-site cysteine to serine results in the decrease in k_{cat} of oxidative phosphorylation by 23,000 times. The K_m however remains similar as there are no drastic changes in the geometry of the active site that will lead to decreased affinity for the ligand. In fact, a new H-bonding interaction develops between the C2 hydroxyl group and OG of serine (Fig. 3a). The poor nucleophilicity of the hydroxyl group of the serine residue in comparison with the cysteinyl sulfur results in drastic diminution in activity of the mutant. The C151G mutant was completely inactive. In the case of H178N, no significant difference is observed in the K_m values of G3P, phosphate, and NAD^+. This is quite expected as His178 is not directly involved in the binding of these ligands. It verifies that the mutation does not induce local perturbation of the active site that can

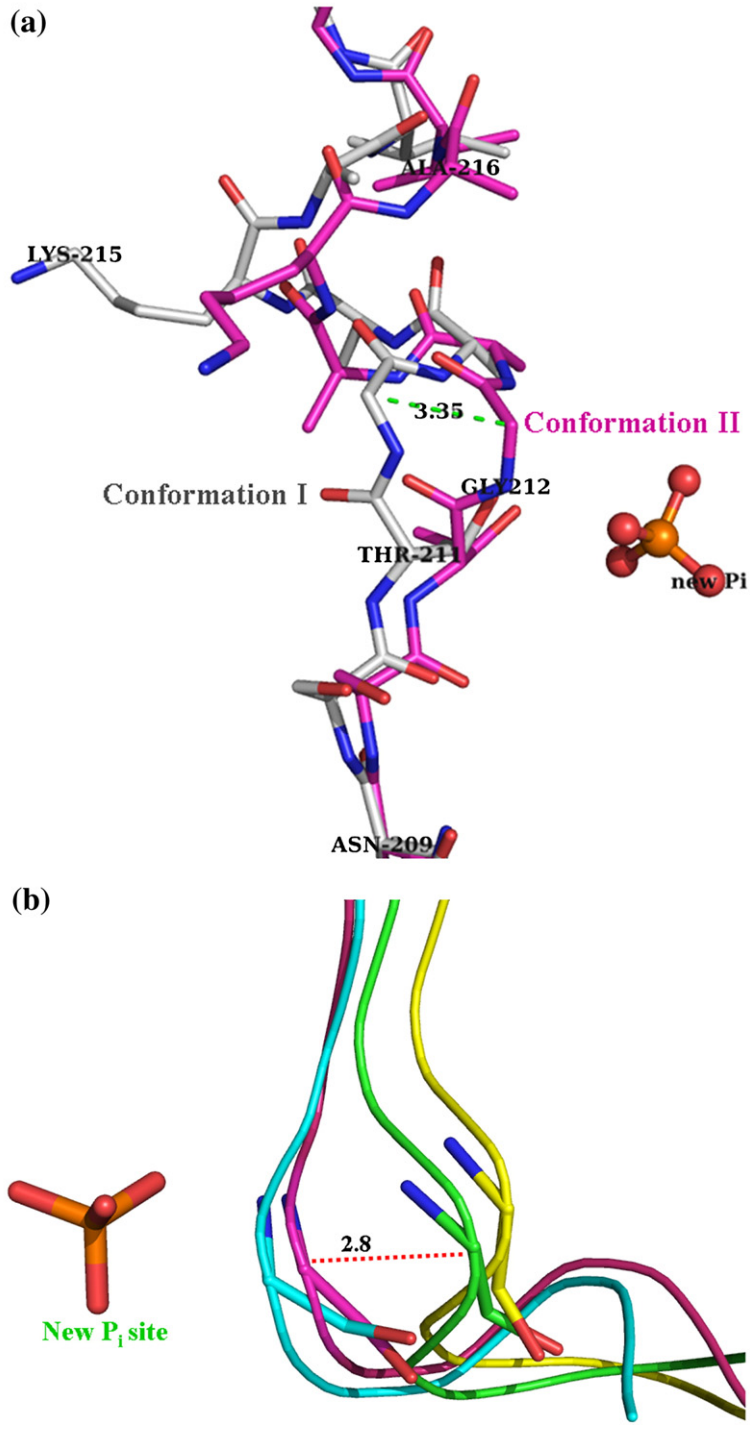

Fig. 6. Conformation of the 209–215 loop. (a) The 209–215 loop exists in two alternate conformations—Conformation I (white) and Conformation II (purple). Conformation I is present in all the structures of SaGAPDH1 except SaGAPDH1-P_A and thioacyl intermediate where it is present in Conformation II. C^{α} of Gly212 in Conformation I moves outward by 3.35 Å than that in Conformation II. The nearby "new P_i" is shown in ball and sticks. This figure presents the superimposed view of the O subunit of SaGAPDH1-P_H (white) with that of SaGAPDH1-P_A (purple). (b) Superposition of the 209–215 loop (O subunit) of SaGAPDH1-P_H (green) and SaGAPDH1-P_A (cyan) with the 206–212 loop (O subunit) of the thioacyl intermediate from BsGAPDH (PDB code: 3CMC). The loop in 3CMC exists both in Conformation A (yellow) and in Conformation B (magenta). Corresponding glycine residues in all the loops have been shown as sticks. Gly212 (C^{α}) in SaGAPDH1-P_H is away by 2.80 Å from corresponding Gly212 (C^{α}) (Conformation B) in BsGAPDH. Thus, the stabilizing interaction between the Gly212 and the "new P_i" phosphate is lost in SaGAPDH1-P_H.

interfere with substrate binding. However, the mutation results in the reduction of k_{cat} of oxidative phosphorylation by 1400 times. Such drastic reduction in the rate obviously raises the question whether the mutation has changed the rate-determining step. In the case of the double mutant, C151S+H178N, the rate of the forward reaction is decreased by 47,000 times with similar affinity for the substrate and the coenzyme. Clearly, the catalytic mechanism is rather complex and identification of true rate-determining step requires the use of D-[1-^{2}H]G3P.

Discussion

This study describes the structure of SaGAPDH1 with a focus to delineate the catalytic mechanism of this "old but still imperfectly known" enzyme. SaGAPDH1 is a phosphorylating D-GAPDH. NAD^+, being its coenzyme, binds to the Rossmann fold of the coenzyme binding domain of the enzyme in an anti conformation. In contrast to BsGAPDH,[27] NAD^+ increases the distance between the two catalytic residues Cys151 and His178. The shortening of this distance in BsGAPDH can be attributed to

Table 2. Kinetic parameters: comparison of the catalytic properties of wild type and mutant SaGAPDH1s

	K_m (G3P) (mM)	K_m (NAD^+) (mM)	K_m (PO_4^{3-}) (mM)	k_{cat} (s^{-1})
Wild type	0.31	316.0	2.54	70.0
C151S	0.34	322.0	3.09	0.09
H178N	0.32	320.0	3.03	0.05
C151S + H178N	0.34	312.0	3.68	0.002

form a reactive thiolate species from catalytic Cys149, enhancing its nucleophilicity during catalysis. However, in our case, the two catalytic residues Cys151 and His178 are already near enough to each other to form a competent thiol nulceophile. Thus, it can be firmly concluded that NAD^+ binding does not affect the catalytic changes of the protein. Mutation of Cys151 to serine resulted in a dramatic decrease of catalytic efficiency of the enzyme though crystal structure of C151S is in conformation with the formation of a Ser^-His^+ ion pair (3HQ4). Kinetic analyses confirm that the active site of phosphorylating SaGAPDH1 is not designed to increase the nucleophilicity of the serine residue. This is in contrast to serine proteases where formation of an ion pair in the catalytic triad is responsible for enhanced nucleophilicity of the catalytically active serine.[28] Mutation of the catalytic cysteine to glycine increases the size of the active-site pocket by almost 10.0 $Å^3$ (3K9Q). The distance between catalytic Cys151 and Asn178 in H178N (3LC1) and C151S + H178N (3KSD) increases to 4.90 and 5.20 Å, respectively. The amide side chain of Asn178 in H178N and C151S + H178N is oriented in a direction away from the imidazole ring of His178. All the other interactions remain unperturbed except the stabilizing interaction of OG of Ser151 with NE2 of His178 ruling out the formation of more nucleophilic hydroxylate species. This is also reflected in its kinetic parameters. In contrast to BsGAPDH,[24] orientation of the 209–215 loop is similar in all the active-site mutants of SaGAPDH1 when compared to the wild-type holoenzyme. Hence, the "new P_i" site in all the mutants is still structurally efficient to bind the phosphate or its analogues even though they are empty because of the crystallization conditions and purification protocol used. The enzyme has two distinct phosphate binding sites: the "classical P_s" site where it binds the substrate phosphate of G3P and the "new P_i" site that is identical with one obtained in TmGAPDH.[21] The presence of both the "P_s" and "new P_i" sites towards the protein surface may account for higher temperature factors of the phosphate ions. However, the average *B*-factor of the "P_s" phosphate is lower than that of the "P_i" phosphate, which indicates the higher flexibility of the latter. SaGAPDH1-P_H has fully occupied "P_s" and the "new P_i" sites, while the "P_s" sites in SaGAPDH1-P_A are occupied by water molecules, unambiguously asserting the fact that NAD^+ contributes to the formation of the "P_s" site. The position of the "P_i" site is a subject of debate and its "true location" depends on the conformation of the strand–loop helix segment containing the amino acid residues 206–212. This loop, corresponding to residues 209–215, is found in Conformation I in all the structures described here except in the SaGAPDH1-P_A and thioacyl intermediate where it adopts Conformation II. The average temperature factors of this segment in both the conformations are comparable, indicating that both of them are stable conformations.

With an aim of better understanding the true intermediates involved in the reaction, we have also solved and analyzed the structures of the binary complexes of the mutants (C151S.NAD, C151G.NAD, and C151S + H178N.NAD) and corresponding ternary complexes with G3P. The structures of ternary complexes are probable representatives of the ground-state Michaelis complex. Apart from the ternary complex of C151G where G3P binds in an inverted manner, the other complexes have the substrate bound in a noncovalent manner with the C3 phosphate positioned in the "P_s" site. This suggests a better affinity of the ligand for the "P_s" site than for the "P_i" site. This conclusion of better affinity for the "P_s" site can apparently contradict the observation that SaGAPDH1-P_H has fully occupied "P_s" and "P_i" sites. However, it is notable that the structure was determined from crystals where the protein was purified with phosphate buffer, which obviously gives the enzyme enough time to bind phosphate ions in "new P_i" sites as well. A quick soaking of the holoenzyme crystal (protein purified from Tris buffer) results in a fully occupied "P_s" site but a vacant "new P_i" site (data not shown). This clearly justifies the observation found in the Michaelis complex. From the structures of the ternary complexes, it is evident the C3P group of the ligand is positioned in the "P_s" site in the ground-state noncovalent Michaelis complexes. These results are however a bit surprising because former studies have pointed out the involvement of the "P_i" site in the catalytic mechanism of GAPDHs.[6] Thus, to elucidate the catalytic mechanism unambiguously, we have solved the structure of thioacyl intermediate with the phosphate group of substrate positioned in the "new P_i site" while the "P_s" site remains totally empty. Oxygen atom at C1 points opposite to His178 disrupting the alignment between itself and NE2 of His178 (Fig. 5c). In comparison to the Michaelis complex, active-site conformation remains almost unperturbed except the 209–215 loop that is found in Conformation I in the ternary complexes but in Conformation II in the thioacyl intermediate.

Catalytic mechanism inferred from structures of SaGAPDH1

The catalytic mechanism obtained from structural and functional investigation of SaGAPDH1 follows the "flip-flop" model for G3P. D-G3P initially binds to the active site with its C3 phosphate positioned in the conserved "P_s" site. It is stabilized by neighboring NAD^+. The binding cavity is mostly formed by basic amino acid residues (Supplementary Fig. 3).

The carbonyl carbon (C1) of D-G3P undergoes a nucleophilic attack by the thiol group of Cys151 to form a hemithioacetal intermediate (Fig. 7, Step I). The reaction occurs through the hydrated (gem-diol) form of G3P (Fig. 7a). Nucleophilicity of the thiol group is initially activated by neighboring catalytically active His178 forming an ion pair. The electrostatic interaction between the oxyanion of the hemithioacetal intermediate (at the reaction pH) and the formal positive charge on the nitrogen atom (N1) of the nicotinamide ring stabilizes the tetrahedral transition state of the reaction.

This is followed by a hydride transfer from C1 of bound G3P to the C4 atom of the nicotinamide ring of bound NAD^+ (Fig. 7, Step II). This hydride transfer is assisted by His178, which plays the univocal role of a general base catalyst. A hydride transfer from C1 of G3P to the C4 atom of the nicotinamide ring of NAD^+ oxidizes the substrate with the formation of a thioacylenzyme intermediate while NAD^+ is reduced to NADH (Fig. 7c). The tetrahedral geometry of the sp^3 hybridized C1 atom of the hemithioacetal is altered to a planar disposition of sp^2 hybridized C1 in the thioacyl complex with SCO and SCC bond angle of 114.82° and 134.07°. Stereochemical prerequisites of the hydride transfer process positions C1–O1 bond, NE2 of His178, and the C4 of the nicotinamide ring in an orientation where the C1–O1 bond is stabilized by NE2 of His178 (Fig. 7b). Formation of the thiaocyl complex by soaking the apoenzyme with G3P is a bit surprising because the coenzyme that is the acceptor of the hydride ion is absent here. It is a well-known fact that the electrophilic carbonyl carbon of aldehyde is a potent acceptor of hydride ion.[29,30] In the case of apo SaGAPDH1, the crystal has been soaked with excess of the substrate. Hence, it can be well ascertained that in the absence of NAD^+, the excess aldehyde is reduced to the corresponding alcohol by accepting the liberated hydride ion.

The thioacyl intermediate then undergoes conformational alterations in such a way that the C3 phosphate, which is still bound to the "P_s" site, "flips" to the empty "new P_i" site (Fig. 7, Step III), and the C1–O1 bond points away from NE2 of His178 (Fig. 7d). This involves a rotation of the O1–C1–C2–O2 plane by ~180° with a C2–C3 bond rotation to position the C3 phosphate in the "new P_i" site. The intermediate was isolated at this stage of reaction. However, we are not certain whether the hydride transfer and flipping of the C3 phosphate are concerted. It can be assumed that the hydride transfer precedes flipping because a hydride transfer with the C3 phosphate of substrate positioned at the "P_s" site can be stabilized by interacting with the substrate. However, this can only be unambiguously ascertained if the thioacyl intermediate would have contained bound NAD^+. The flipping of the C3 phosphate is followed by the release of NADH. As the thioacyl intermediate discussed here is devoid of the coenzyme, the factors that can trigger the exchange of NADH with a new NAD^+ molecule are only speculative. However, superimposition of the intermediate with the Michaelis complex (Fig. 5c) leads us to postulate the disruption of the hydrogen-bonding interaction between O2D and the oxygen atom of the C3 phosphate and the disruption of water-mediated stabilization of O3D with C2–OH may be some of the contributing factors that destabilize the ground state of the reaction. The C2–OH is now hydrogen bonded with the protonated NE2 of His178 (Fig. 7d).

The phosphorolysis step needs the assistance of His178 that again acts as a general acid catalyst as it does in acylation step. This necessitates repositioning of the C1–O1 bond in a favorable orientation with respect to NE2 of His178. Exchange of coenzyme takes place. NADH is released from the enzyme and a new NAD^+ enters. Entry of a new NAD^+ molecule again flips back or "flops" the C3 phosphate from the "new P_i site" to the initial "P_s" site so that the C1–O1 bond now gets the optimal orientation for assistance by His178 (Fig. 7, Step IV). The stabilizing interactions between O2D and the C3 phosphate and that between O3D and C2–OH are again restored (Fig. 7e). Finally, the C1 atom of the thioacyl intermediate undergoes a nucleophilic attack by the inorganic phosphate (Fig. 7, Step IV), leading to formation of 1,3-BPG (Fig. 7f).

Different crystal structures of the wild-type enzyme in apo and holo forms, binary complexes of active-site mutants (C151S.NAD, C151G.NAD, H178N.NAD, and C151S+H178N.NAD), the corresponding ternary complexes with substrate (C151S.NAD.G3P, C151G.NAD.G3P, and C151S+H178N.NAD.G3P), and thioacyl intermediate have been discussed. A new anion recognition site, the "new P_i" site, is obtained. A new conformation of the 209–215 loop has also been identified. Ternary complexes present here are representatives of noncovalent Michaelis complexes in the ground state. D-G3P binds to the C151G mutant in an inverted manner. Inferences drawn from the analysis of the acylated intermediate in comparison with the Michaelis complexes suggest the "flip-flop" model proposed for the enzyme mechanism.[25]

Further work can be carried out to determine and characterize the structure of the hemithioacetal and thioacyl intermediate in the presence of NAD^+, which will definitely give a more detailed view of the catalytic mechanism. The driving force behind the phosphorolysis step and the exact site of location of the inorganic phosphate is still speculative. Trapping of the Michaelis complex with the product can give further insights into the complex reaction mechanism.

Materials and Methods

Materials

All the enzymes used in molecular biology works were from Fermentas. D,L-G3P and NAD^+ were purchased from

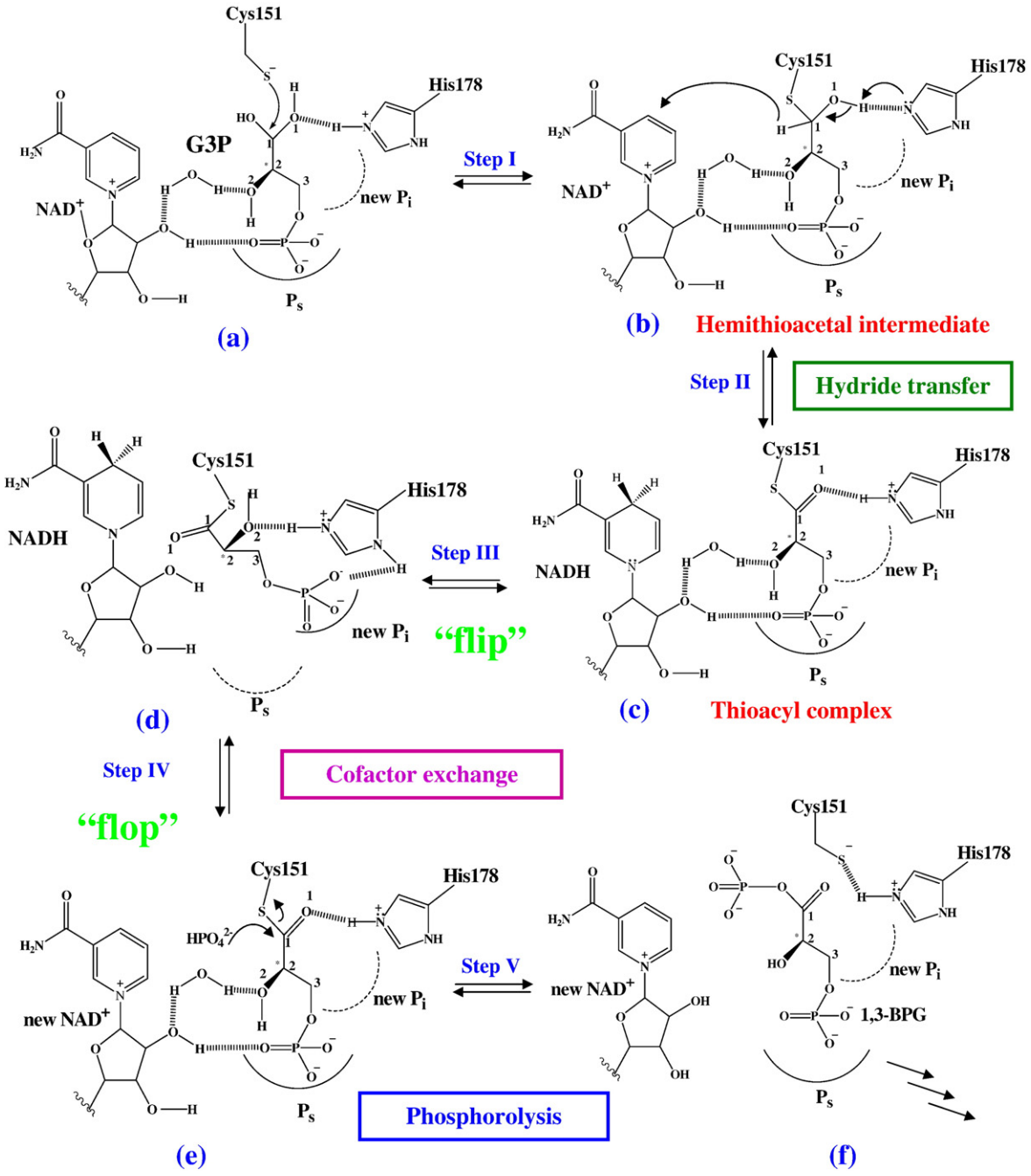

Fig. 7. Catalytic mechanism inferred from structures of SaGAPDH1: Step I: D-G3P initially binds to the active site with its C3 phosphate positioned in the "P_s" site (a). Nucleophilic thiolate form of Cys151 attacks C1 atom of D-G3P leading to a formation of a tetrahedral hemithioacetal intermediate (b). Step II: Hydride transfer occurs from C1 of D-G3P to the C4 atom of the nicotinamide ring of NAD^+. This results in the oxidation of the hemithioacetal intermediate to a thioacyl complex with a concomitant reduction of NAD^+ to NADH. The C3 phosphate of D-G3P is still bound to the "P_s" site while the "new P_i" site is empty (c). The phosphate in the "P_s" site is held by tight interactions with NAD^+. The acyl carbonyl is stabilized by hydrogen bonding with the protonated NE2 of His178. Step III: Hydride transfer is followed by "flipping" of C3 phosphate to the "new P_i" site (d). The C1–O1 bond now points away from His178. The hydroxyl group at C2 is in turn stabilized by His178. O1 and O2 point opposite to each other. Step IV: Cofactor exchange occurs. A new NAD^+ enters the active site. The thioacyl complex again flips back or "flops" to relocate the C3 phosphate in the "P_s" position. The hydrogen-bonding interactions of the C3 phosphate with the new NAD^+ are restored. Step V: Finally, inorganic phosphate phosphorylates the C1 carbon forming the desired product, 1,3-BPG (f). During phosphorolysis, the electrophilicity of acyl carbon is enhanced by the general acid catalyst His178. 1,3-BPG is released from active site and the enzyme becomes ready to incorporate a new substrate molecule. C2 of D-G3P is chiral and marked with an asterisk (*). Its absolute configuration is R and is retained throughout the process.

Sigma Chemicals. Other reagents and chemicals used were of analytical grade.

Overexpression, purification, and crystallization

Cloning, overexpression, purification, and crystallization of the wild-type SaGAPDH1 in apo and holo forms have been previously described.[31,32] The apo form was obtained from holenzyme by activated charcoal treatment.[31] To obtain phosphate-bound proteins, we used 50 mM phosphate buffer in the final gel-exclusion chromatography. Active-site mutants C151S, C151G, and H178N were generated using overlap extension method[33] and confirmed by automated DNA sequencing. The primers used are listed (Supplementary Table 1). NAD^+ was bound to all the mutants such as the wild type, and the mutants were all purified and crystallized as binary complexes with NAD^+ (C151S.NAD, C151G.NAD, H178N.NAD, and C151S+H178N.NAD). Glycerol [5% (v/v)] was added to the buffers used for purification of mutants. The wild-type holoenzyme and apoenzyme crystallized from 0.1 M Tris–HCl, pH 8.5, and 20% (w/v) PEG 4000 at 277 K and from 0.1 M Tris–HCl, pH 8.2, and 32% (w/v) PEG 3350 at 298 K, respectively. Crystals of SaGAPDH1-P_H and SaGAPDH1-P_A were obtained at 298 K from 0.1 M Tris–HCl, pH 8.5, and 25% (w/v) PEG 4000 and from 0.1 M Tris–HCl, pH 8.7, and 32% (w/v) PEG 3350, respectively. Crystals of active-site mutants (binary complexes) C151S.NAD, C151G.NAD, and C151S+H178N.NAD grew at 298 K from 0.1 M Tris–HCl, pH 8.5, and 28% (w/v) PEG 4000, from 0.1 M Tris–HCl, pH 8.2, and 30% (w/v) PEG 4000, and from 0.1 M Tris–HCl, pH 8.5, and 30% (w/v) PEG 4000, respectively, while H178N.NAD crystallized from 0.1 M Tris–HCl, pH 8.2, and 30% (w/v) PEG 4000 at 277 K. To obtain ternary complexes (C151S.NAD.G3P, C151G.NAD.G3P, and C151S+H178N.NAD.G3P), we soaked crystals of corresponding binary complexes with 50 mM D,L-G3P in reservoir solution for 10 min. The thioacyl intermediate of the apoenzyme was obtained by soaking the crystals of apoenzyme quickly with 50 mM G3P for 1–2 min.

Data collection and structure determination

All the diffraction data were collected at our home source equipped with a Rigaku R Axis IV++ detector with Cu Kα X-rays (1.5418 Å) generated by a Rigaku Micromax HF007 Microfocus rotating anode X-ray generator. The crystals were cryoprotected[34] with glycerol (percentage varied depending upon the crystallization conditions) and flash cooled in liquid nitrogen stream at 100 K. Data were processed with d*TREKv9.8.[35] Data collection statistics are detailed in Table 1. The intensities were converted into the corresponding structure factors using TRUNCATE.[36] The structure of wild-type SaGAPDH1 was solved by molecular replacement using MOLREP[37] within the CCP4 package.[38] TmGAPDH (PDB entry: 1HDG)[21] with an identity of 53% was used as the starting model. A promising solution was obtained similar to the results obtained from Auto-Rickshaw.[39] The initial solution obtained was subjected to cycles of rigid-body refinement to generate the $2F_o-F_c$ and F_o-F_c map followed by consecutive cycles of TLS and restrained refinement in Refmac5[40] until a map with interpretable electron density was obtained. Cycles of restrained refinement alternated with manual model building in Coot[41] to improve the quality of the model. After the preliminary refinement of the polypeptide chain, the ligands were placed unambiguously according to the difference electron maps calculated at this stage. This was ultimately followed by modeling the solvent molecules. Each peak contoured at 3 σ in the F_o-F_c map was identified as the water molecule, taking into consideration their geometrical constraints as well. The progress of the refinement was monitored by a steady decrease and convergence of R and R_{free}[42] values. The stereochemical quality of the model was validated using PROCHECK.[43]

The structures of the apoenzyme, thioacyl intermediate, binary complexes, and the ternary complexes were determined by difference Fourier maps phased using the atomic coordinates of the wild-type structure of SaGAPDH1 in holo form. Model building was done in Coot and refinement was done in Refmac5 in a manner similar to the wild-type enzyme. The structure of NAD^+ was taken from the Refmac library while the structures of D-G3P (aldehyde and gem-di-ol form) were drawn in PRODRG.[44] All of them were fitted in the electron density maps using ARP/wARP ligand.[45] Refinement statistics are listed in Table 1.

Structure homologues to SaGAPDH1 in PDB were searched by the BLASTP server.[46] Structure superpositions were done using LSQKAB,[47] and interface analysis and accessible surface area calculations were done using PISA.[48] Figures 1–6 are generated by PyMOL[49] and Fig. 7 is generated by ChemDraw Ultra Version 6.0†. Simulated annealing F_o-F_c omit maps were generated using CNS.[50]

Kinetic analyses

The kinetic analyses were performed according to the method of Ferdinand.[51] Rate measurements were carried out in a Thermo Scientific Spectrophotometer by monitoring the change in absorbance at 340 nm due to NADH formation. It has been standardized that the pH optimum and the temperature of maximum activity for the wild-type enzyme is 8.7 and 25 °C. Thus, all the kinetic experiments of the wild type and the mutants were done at 25 °C at pH 8.7. Reaction mixture (500 μL) contained 40 mM triethanol amine, 2 mM ethylenediaminetetraacetic acid, and 50 mM K_2HPO_4, pH 8.7. Michaelis–Menten parameters, K_m, and V_{max} are obtained from nonlinear regression fit of the kinetic data using GraphPad Prism 4.00.[52] All K_m values were determined at saturating concentrations of other substrates. The turnover number (k_{cat}) was calculated using molar extinction coefficient of 22,920 M^{-1} cm^{-1} at 280 nm.[53] The buffers used to determine the pH optimum for the maximum activity are 2-(*N*-morpholino) ethanesulfonic acid (pH 5.0–6.5), triethanol amine (pH 7.0–9.0), and glycine (pH 9.5–10.5).

PDB accession numbers

Coordinates and structure factor amplitudes have been submitted in the PDB under the accession codes 3LVF (holoenzyme), 3LC7 (apoenzyme), 3K73 (phosphate-bound holoenzyme—SaGAPDH1-P_H), 3L6O (phosphate-bound apoenzyme—SaGAPDH1-P_A), 3HQ4 (C151S.NAD), 3K9Q (C151G.NAD), 3LC1 (H178N.NAD), 3KSD (C151S+H178N.NAD), 3KV3 (C151S.NAD.G3P), 3L4S (C151G.NAD.G3P), 3KSZ (C151S+H178N.NAD.G3P), and 3LC2 (thioacyl intermediate).

† http://www.cambridgesoft.com

Acknowledgements

The authors like to acknowledge the Department of Biotechnology, Government of India, for financial assistance and setting up the crystallographic facility at the Indian Institute of Technology (IIT) Kharagpur. S.M. thanks the Council of Scientific and Industrial Research for individual fellowship. The authors gratefully acknowledge the Central Research Facility of IIT Kharagpur. The authors thank Mr. Sudipta Bhattacharyya (Department of Biotechnology, IIT Kharagpur) and Mr. Kaushik Chandra and Mr. Sayantan Mondal (Department of Chemistry, IIT Kharagpur) for helpful discussions. The genomic DNA of MRSA252 was a kind gift from Dr. H. G. Wiker, University of Bergen.

Supplementary Data

Supplementary data associated with this article can be found, in the online version, at doi:10.1016/j.jmb.2010.07.002

References

1. Menichetti, F. (2005). Current and emerging serious Gram-positive infections. *Clin. Microbiol. Infect.* **11**, 22–28.
2. Hiramatsu, K., Hanaki, H., Ino, T., Yabuta, K., Oguri, T. & Tenover, F. C. (1997). Methicillin-resistant *Staphylococcus aureus* clinical strain with reduced vancomycin susceptibility. *J. Antimicrob. Chemother.* **40**, 135–136.
3. Segal, H. L. & Boyer, P. D. (1953). The role of sulfhydryl groups in the activity of D-glyceraldehyde 3-phosphate dehydrogenase. *J. Biol. Chem.* **204**, 265–281.
4. Trentham, D. R. (1971). Reactions of D-glyceraldehyde 3-phosphate dehydrogenase facilitated by oxidized nicotinamide–adenine dinucleotide. *Biochem. J.* **122**, 59–69.
5. Soukri, A., Mougin, A., Corbier, C., Wonacott, A., Branlant, C. & Branlant, G. (1989). Role of the histidine 176 residue in glyceraldehyde-3-phosphate dehydrogenase as probed by site-directed mutagenesis. *Biochemistry*, **28**, 2586–2592.
6. Michels, S., Rogalska, E. & Branlant, G. (1996). Phosphate-binding sites in phosphorylating glyceraldehyde-3-phosphate dehydrogenase from *Bacillus stearothermophilus*. *FEBS J.* **235**, 641–647.
7. Boschi-Muller, S. & Branlant, G. (1999). The active site of phosphorylating glyceraldehyde-3-phosphate dehydrogenase is not designed to increase the nucleophilicity of a serine residue. *Arch. Biochem. Biophys.* **363**, 259–266.
8. Moras, D., Olsen, K. W., Sabesan, M. N., Buehner, M., Ford, G. C. & Rossmann, M. G. (1975). Studies of asymmetry in the three-dimensional structure of lobster D-glyceraldehyde-3-phosphate dehydrogenase. *J. Biol. Chem.* **250**, 9137–9162.
9. Pancholi, V. & Fischetti, V. A. (1992). A major surface protein on group A streptococci is a glyceraldehyde-3-phosphate-dehydrogenase with multiple binding activity. *J. Exp. Med.* **176**, 415–426.
10. Delgado, M. L., O'Connor, J. E., Azorin, I., Renau-Piqueras, J., Gil, M. L. & Gozalbo, D. (2001). The glyceraldehyde-3-phosphate dehydrogenase polypeptides encoded by the *Saccharomyces cerevisiae* TDH1, TDH2 and TDH3 genes are also cell wall proteins. *Microbiology*, **147**, 411–417.
11. Gozalbo, D., Gil-Navarro, I., Azorin, I., Renau-Piqueras, J., Martinez, J. P. & Gil, M. L. (1998). The cell wall-associated glyceraldehyde-3-phosphate dehydrogenase of *Candida albicans* is also a fibronectin and laminin binding protein. *Infect. Immun.* **66**, 2052–2059.
12. Zang, W. Q., Fieno, A. M., Grant, R. A. & Yen, T. S. (1998). Identification of glyceraldehyde-3-phosphate dehydrogenase as a cellular protein that binds to the hepatitis B virus posttranscriptional regulatory element. *Virology*, **248**, 46–52.
13. Modun, B. & Williams, P. (1999). The staphylococcal transferrin-binding protein is a cell wall glyceraldehyde-3-phosphate dehydrogenase. *Infect. Immun.* **67**, 1086–1092.
14. Taylor, J. M. & Heinrichs, D. E. (2002). Transferrin binding in *Staphylococcus aureus*: involvement of a cell wall-anchored protein. *Mol. Microbiol.* **43**, 1603–1614.
15. Sirover, M. A. (1999). New insights into an old protein: the functional diversity of mammalian glyceraldehyde-3-phosphate dehydrogenase. *Biochim. Biophys. Acta*, **1432**, 159–184.
16. Didierjean, C., Corbier, C., Fatih, M., Favier, F., Boschi-Muller, S., Branlant, G. & Aubry, A. (2003). Crystal structure of two ternary complexes of phosphorylating glyceraldehyde-3-phosphate dehydrogenase from *Bacillus stearothermophilus* with NAD and D-glyceraldehyde 3-phosphate. *J. Biol. Chem.* **278**, 12968–12976.
17. Skarzyński, T., Moody, P. C. & Wonacott, A. J. (1987). Structure of holo-glyceraldehyde-3-phosphate dehydrogenase from *Bacillus stearothermophilus* at 1.8 Å resolution. *J. Mol. Biol.* **193**, 171–187.
18. Weber, H., Engelmann, S., Becher, D. & Hecker, M. (2004). Oxidative stress triggers thiol oxidation in the glyceraldehyde-3-phosphate dehydrogenase of *Staphylococcus aureus*. *Mol. Microbiol.* **52**, 133–140.
19. Shenton, D. & Grant, C. M. (2003). Protein S-thiolation targets glycolysis and protein synthesis in response to oxidative stress in the yeast *Saccharomyces cerevisiae*. *Biochem. J.* **374**, 513–519.
20. Buehner, M., Ford, G. C., Moras, D., Olsen, K. W. & Rossmann, M. G. (1974). Structure determination of crystalline lobster D-glyceraldehyde-3-phosphate dehydrogenase. *J. Mol. Biol.* **82**, 563–585.
21. Korndörfer, I., Steipe, B., Huber, R., Tomschy, A. & Jaenicke, R. (1995). The crystal structure of holo-glyceraldehyde-3-phosphate dehydrogenase from the hyperthermophilic bacterium *Thermotoga maritima* at 2.5 Å resolution. *J. Mol. Biol.* **246**, 511–521.
22. Cook, W. J., Senkovich, O. & Chattopadhyay, D. (2009). An unexpected phosphate binding site in glyceraldehyde 3-phosphate dehydrogenase: crystal structures of apo, holo and ternary complex of *Cryptosporidium parvum* enzyme. *BMC Struct. Biol.* **9**, 9.
23. Corbier, C., Della Seta, F. & Branlant, G. (1992). A new chemical mechanism catalysed by a mutated aldehyde dehydrogenase. *Biochemistry*, **31**, 12532–12535.
24. Didierjean, C., Corbier, C., Fatih, M., Favier, F., Boschi-Muller, S., Branlant, G. & Aubry, A. (2003). Crystal structure of two ternary complexes of phosphorylating glyceraldehyde-3-phosphate dehydrogenase from *Bacillus stearothermophilus* with NAD and D-glyceraldehyde 3-phosphate. *J. Biol. Chem.* **278**, 12968–12976.

25. Moniot, S., Bruno, S., Vonrhein, C., Didierjean, C., Boschi-Muller, S., Vas, M. *et al.* (2008). Trapping of the thioacylglyceraldehyde-3-phosphate dehydrogenase intermediate from *Bacillus stearothermophilus*. Direct evidence for a flip-flop mechanism. *J. Biol. Chem.* **283**, 21693–21702.
26. Yun, M., Park, C. G., Kim, J. Y. & Park, H. W. (2000). Structural analysis of glyceraldehyde 3-phosphate dehydrogenase from *Escherichia coli*: direct evidence of substrate binding and cofactor-induced conformational changes. *Biochemistry*, **35**, 10702–10710.
27. Skarzyński, T. & Wonacott, A. J. (1988). Coenzyme-induced conformational changes in glyceraldehyde-3-phosphate dehydrogenase from *Bacillus stearothermophilus*. *J. Mol. Biol.* **203**, 1097–1118.
28. Kuhn, P., Knapp, M., Soltis, S. M., Ganshaw, G., Thoene, M. & Bott, R. (1998). The 0.78 Å structure of a serine protease: *Bacillus lentus* subtilisin. *Biochemistry*, **37**, 13446–13452.
29. Nystroman, R. F. & Brown, W. G. (1947). Reduction of organic compounds by lithium aluminum hydride. I. Aldehydes, ketones, esters, acid chlorides and acid anhydrides. *J. Am. Chem. Soc.* **69**, 1197–1199.
30. Finar, I. L. (1973). *Monohydric Alcohols. Organic Chemistry*, vol. I, 6th edit, pp. 176–194. Longman Scientific and Technical, Essex, England.
31. Mukherjee, S., Saha, B., Dutta, D. & Das, A. K. (2010). Purification, crystallization and preliminary X-ray analysis of apo glyceraldehyde-3-phosphate dehydrogenase 1 (GAP1) from methicillin resistant *Staphylococcus aureus* (MRSA252). *Acta Crystallogr., Sect. F: Struct. Biol. Cryst. Commun.* **66**, 506–508.
32. Mukherjee, S., Dutta, D., Saha, B. & Das, A. K. (2008). Expression, purification, crystallization and preliminary X-ray diffraction studies of glyceraldehyde-3-phosphate dehydrogenase 1 from methicillin-resistant *Staphylococcus aureus* (MRSA252). *Acta Crystallogr., Sect. F: Struct. Biol. Cryst. Commun.* **64**, 929–932.
33. Ho, S. N., Henry, D. H., Horton, R. M., Pullen, J. K. & Peasea, L. R. (1989). Site-directed mutagenesis by overlap extension using the polymerase chain reaction. *Gene*, **77**, 51–59.
34. Teng, T. Y. (1990). Mounting of crystals for macromolecular crystallography in a free-standing thin film. *J. Appl. Crystallogr.* **23**, 387–391.
35. Pflugrath, J. W. (1999). The finer things in X-ray diffraction data collection. *Acta Crystallogr., Sect. D: Biol. Crystallogr.* **55** , 1718–1725.
36. French, G. S. & Wilson, K. S. (1978). On the treatment of negative intensity observations. *Acta Crystallogr., Sect. A: Cryst. Phys., Diffr., Theor. Gen. Crystallogr.* **34**, 517–525.
37. Vagin, A. & Teplyakov, A. (1997). MOLREP: an automated program for molecular replacement. *J. Appl. Crystallogr.* **30**, 1022–1025.
38. Collaborative Computational Project, Number 4. (1994). The CCP4 suite: programs for protein crystallography. *Acta Crystallogr., Sect. D: Biol. Crystallogr.* **50**, 760–763.
39. Panjikar, S., Parthasarathy, V., Lamzin, V. S., Weiss, M. S. & Tucker, P. A. (2005). Auto-Rickshaw: an automated crystal structure determination platform as an efficient tool for the validation of an X-ray diffraction experiment. *Acta Crystallogr., Sect. D: Biol. Crystallogr.* **61**, 449–457.
40. Murshudov, G. N., Vagin, A. A. & Dodson, E. J. (1997). Refinement of macromolecular structures by the maximum-likelihood method. *Acta Crystallogr., Sect. D: Biol. Crystallogr.* **53**, 240–255.
41. Emsley, P. & Cowtan, K. (2004). Coot: model-building tools for molecular graphics. *Acta Crystallogr., Sect. D: Biol. Crystallogr.* **60**, 2126–2132.
42. Brünger, A. T. (1992). Free *R* value: a novel statistical quantity for assessing the accuracy of crystal structures. *Nature*, **355**, 472–475.
43. Laskowski, R. A., MacArthur, M. W., Moss, D. S. & Thornton, J. M. (1993). PROCHECK: a program to check the stereochemical quality of protein structures. *J. Appl. Crystallogr.* **26**, 283–291.
44. Schüttelkopf, A. W. & van Aalten, D. M. (2004). PRODRG: a tool for high-throughput crystallography of protein–ligand complexes. *Acta Crystallogr., Sect. D: Biol. Crystallogr.* **60**, 1355–1363.
45. Evrard, G. X., Langer, G. G., Perrakis, A. & Lamzin, V. S. (2007). Assessment of automatic ligand building in ARP/wARP. *Acta Crystallogr., Sect. D: Biol. Crystallogr.* **63**, 108–117.
46. Altschul, S. F., Thomas, L. M., Alejandro, A. S., Zhang, J., Zhang, Z., Miller, W. & Lipman, D. J. (1997). Gapped BLAST and PSI-BLAST: a new generation of protein database search programs. *Nucleic Acids Res.* **25**, 3389–3402.
47. Kabsch, W. (1976). A solution for the best rotation to relate two sets of vectors. *Acta Crystallogr., Sect. A: Cryst. Phys., Diffr., Theor. Gen. Crystallogr.* **32**, 922–923.
48. Krissinel, E. & Henrick, K. (2007). Inference of macromolecular assemblies from crystalline state. *J. Mol. Biol.* **372**, 774–797.
49. DeLano, W. L. (2002). *The PyMOL Molecular Graphics System.* DeLano Scientific LLC, San Carlos, CA; Available at www.pymol.org.
50. Brunger, A. T., Adams, P. D. & Rice, L. M. (1997). New applications of simulated annealing in X-ray crystallography and solution NMR. *Structure*, **5**, 325–336.
51. Ferdinand, W. (1964). The isolation and specific activity of rabbit-muscle glyceraldehyde phosphate dehydrogenase. *Biochem. J.* **92**, 578–585.
52. GraphPad Prism version 4.00 for Windows: GraphPad Software. (2004). San Diego, CA. Available at www.graphpad.com.
53. Gasteiger, E., Hoogland, C., Gattiker, A., Duvaud, S., Wilkins, M. R., Appel, R. D. & Bairoch, A. (2005). Protein identification and analysis tools on the ExPASy server. In *The Proteomics Protocols Handbook* (Walker, J. M., ed.), pp. 571–607, Humana Press, Totowa, NJ.